Quantifying Surface Loss Of Mechanically Polished Silica Cantilevers

Paul Holt Msci

Thesis
submitted to the
University of Glasgow
for the degree of
MSc

UNIVERSITY
of
GLASGOW

Institute for Gravitational Research
Department of Physics & Astronomy
University of Glasgow
Scotland

January 2007

ProQuest LLC.
789 East Eisenhower Parkway
P.O. Box 1346
Ann Arbor, MI 48106 – 1346

To my mother and father, Brenda and Peter, for always being there.

Summary

Materials with a high quality factor are used, for the test mass and suspension elements, in interferometric gravitational wave detectors to reduce off resonance thermal displacement noise. An experiment to increase the quality factor of mechanically polished silica cantilevers by etching their surface is described. An estimation of the thickness of the damaged layer due to polishing is found and we estimate how lossy this layer is. This was achieved by repeatedly etching a cantilever in solution and measuring its mechanical loss in each instance. In this way mechanical loss as a function of etch depth can be determined. This layer was estimated to be 0.5 micron deep with a loss of ϕ_s=2.98 $\times$ 10^{-8} which is three times higher than the surface loss predicted by the current empirical model. This has important implications as the test mass mirrors used in interferometric gravitational wave detectors are comprised of mechanically polished silica. Measurements of single layer dielectric coatings of silica, tantala and doped tantala for use in interferometric gravitational wave detectors is also described. It was found that the silica coating had the lowest level of measured mechanical loss overall at 3.77 $\times$ 10^{-5}. It was also found doped tantala had a lower level of measured loss than tantala, 2.965 $\times$ 10^{-4} in the doped case compared to 4.24 $\times$ 10^{-4}.

Acknowledgements

First it seems only right to thank Professor James Hough for giving me the opportunity to work with the group and for securing my funding. I would also like to thank him for his patience particularly in the initial stages.

Thanks to Dr Stuart Reid for his invaluable help and assistance through the year. Stuart was a very effective mentor: he always challenged my basic assumptions, encouraging me never to take things at face value. He made me a better scientist. I am indebted to him for this and for so much more.

Dr Kiril Tokmakov deserves a great deal of my praise. His patience and good nature made him a perfect laboratory partner. I cannot speak more highly of Kiril as a person. He is eccentric and good humored and these great qualities of his ensured time waiting for results in the laboratory passed quickly.

I must thank Alastair Grant my office mate for allowing me to tap into that seemingly bottomless well of knowledge he posses. I am also glad for his excellent proof reading skills, though all errors that slip through are of course mine.

Dr Alastair Hepstonstall and Alan Cumming deserve recognition for being very approachable and very helpful. Iain Martin deserves my thanks too, especially for all of his assistance in the beginning of the year as I tried to get to grips with the laboratory equipment.

I would also like to extend my gratitude to the technicians: Allan Latta, Colin Craig, Stephen Craig and Neil Robertson. Maybe the workshop is a tidier place now I have left?!

On a more personal note, I would like to thank my close friends Cristiano Sabiu and Eamon Scullion. Thank you for allowing me to pop up to your offices from time to time for a break. What can i say about Eamon? He is one of the closest friends I have ever had. He taught me how deep (or complicated?!) people can be and what can be achieved when someone really is determined. I am sure he will "push through" whatever obstacles lie ahead. I wish Cris all of the best in Portsmouth. I hope he finds people like Eamon and I to spend time with. I wish him good luck for that. Next, I would like to acknowledge the international contingent of my friends: Barbara, Lida and Tod for all those fun times spent together at Kelvinhaugh street. Thanks to Lida for those counseling sessions over coffee (you really should start charging for that Lida!).

Lastly, but most importantly, I would like to thank my mother, father, brother and sister. I don't think it is possible to find a more supportive and understanding family. For that, I will always be blessed.

This research was funded by EPSRC.

Declaration

The work in this thesis is based on research carried out at the Institute for Gravitational Research within the Department of Physics & Astronomy of the University of Glasgow, Scotland. No part of this thesis has been submitted elsewhere for any other degree or qualification and it is all my own work unless referenced to the contrary in the text.

Preface

In Chapter One, the nature of gravitational waves is discussed, together with methods for detection and the factors that limit sensitivity in interferometric schemes.

In Chapter Two, aspects of the theory of thermal noise are discussed and it is shown that, in one model, using materials with a low mechanical dissipation reduces thermal noise away from resonance.

In Chapter Three, investigations into the correlation between etching of a mechanically polished cantilever and the measured mechanical dissipation are discussed. Contribution to the design of the experiment came from J. Hough, S. Reid, V. Mitrofanov, and K. Tokmakov. I was assisted in the laboratory by K. Tokmakov and C. Craig. The analysis of the results was carried out by the author. Valuable conversations were had with S. Reid and K. Tokmakov.

In Chapter Four, investigations into single layer dielectric coatings are discussed. The measurements were done by the author with a contribution from I. Martin. The coating analysis was done by the author in conjunction with S. Reid, S. Rowan and I. Martin. The rest of the analysis was completed by the author.

Contents

List of Figures

List of Tables

Chapter 1

Introduction

1.1 Introduction

One of the most exciting predictions of Einstein's general theory of relativity (1916) is the existence of gravitational waves. In Newtonian mechanics, space-time was regarded as a set of rigid cartesian coordinates against which all events in the universe can be measured. In Einstein's universe, it is an elastic medium that can be warped by the presence of matter and energy. All particles in the universe follow straight lines or geodesics in curved space-time. This accounts for the phenomenon we call gravity.

In General Relativity, space-time is an elastic medium, capable of sustaining waves. It is incredibly stiff so waves in space-time will have to be produced from colossal astrophysical events, and even then they will have a tiny amplitude ($< 10^{-19}$ m). These are gravitational waves and they are produced in a way analogous to the production of electromagnetic waves by accelerating charges, when large masses are accelerated in an asymmetrical way in strong gravitational fields (see e.g. Hough and Rowan, 2000). Gravitational waves are expected to propagate at the speed of light.

Sources expected to produce gravitational waves include: supernova explosions, coalescing compact binaries, black hole- black hole mergers, pulsars etc. The Big Bang also promises to be a source of gravitational waves, producing a stochastic background of gravitational radiation that could exist alongside the cosmic microwave background.

Building detectors capable of "sensing" gravitational waves, although very challenging, is of extreme scientific importance. Gravitational waves may provide us with great insight into the universe and provide further verification of Einstein theory. They may even hint at a more fundamental theory of gravity (Thorne, 1995). The expected revolution of gravitational wave astronomy can be compared to the revolution in the middle of the twentieth century with the development of radio astronomy. This had a profound impact on astronomy. It painted a picture of a far more violent universe than previously thought. It uncovered new phenomena such as pulsars, quasars and the cosmic microwave background. It is hoped that gravitational waves will also open up an new perspective on the universe, because the information is very different (almost "orthogonal to") to the information carried by electromagnetic waves (Thorne, 1995).

1.2 The Nature of Gravitational Waves

This section follows the approach outlined by L Ju et al, (2000). The Einstein equations are a set of 10 coupled differential equations. They describe how matter/energy curves space-time, which in turn determines how matter/energy is distributed and vice versa. Written in the language of tensors they can be expressed in a single form as:

$$\mathrm{T} = \frac{c^4}{8\pi G}\mathrm{G} \tag{1.1}$$

$\boldsymbol{T}$ is the stress energy tensor, $\boldsymbol{G}$ is the Einstein curvature tensor, c is the speed of light

and G is the gravitational constant. The equation is written in this form to draw attention to an analogy with Hooke's Law [1]. $\frac{c^4}{8\pi G}$ plays the role of a coupling constant. In the Newtonian description, the coupling constant is infinite so any changes in a gravitational field propagate instantaneously. However, in relativity it has a finite value and so changes in a gravitational field propagate at a finite speed, the speed of light. The coupling constant has an enormous value, approximately 10^{43}, which explains why newtonian gravity is a good approximation to Einstein's theory in most circumstances. The finite coupling constant implies space-time has an elasticity. It thus capable of supporting waves. These "Gravitational waves" will have a very tiny amplitude, but high energy density (Blair, 2000).

Consider a group of test particles in deep space, arranged in a perfectly spherical configuration (a test particle is an idealized model of an object whose mass is so small that it does not appreciably disturb the ambient gravitational field). The test particles are falling towards a point, the centre of mass of the system. As a consequence of the inverse square law, there is no difference between the gravitational field of a point mass and that of the same mass distributed in a uniform spherical distribution. Therefore, as long as the collapse remains perfectly spherical, there will be no variation in the external gravitational field. Hence there can be no gravitational waves produced. Although this example is through analogy with the Newtonian description of gravity, the result that only the motion of large masses in an asymmetrical way produce gravitational waves holds in the GR case too.

The simplest non-spherical motion is one in which the edge masses move inwards and the top and bottom masses move apart (see figure 1.1). This is the quadrupolar motion of a gravitational wave. Dipolar emission of gravitational waves is not possible due the

[1] Blair Detection of gravitational waves 2005

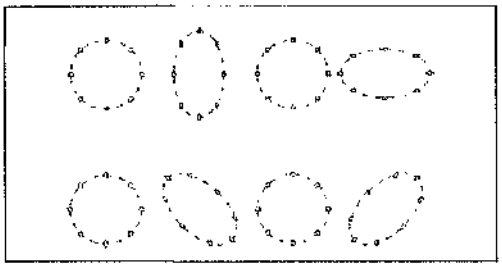

Figure 1.1: This is the effect a gravitational wave has on a ring of test masses. The h_+ polarization is shown by the red particles; the $h_\times$ by the blue.

conservation of angular and linear momentum and the fact there is only one sign of mass. There are two polarizations of gravitational waves: h_+ and $h_\times$ and they exist at 45 degrees the each other.

This distinctive orthogonal "stretching" and "squeezing" of space-time is characteristic of a gravitational wave. It is a time-dependent strain in space. It can be shown that a suitably polarized gravitational wave of amplitude h will produce a strain given by (Robertson, 2000):

$$\frac{\delta L}{L} = \frac{h}{2} \tag{1.2}$$

δL is the change in the separation of two free masses. Measuring this change is the basis of all detectors. The great challenge for the experimental physicist is that these strains in space are expected to be tiny. Even from a nearby supernova, the strain is expected to be 10^{-18} or less . To detect events at a reasonable rate, gravitational wave detectors are being built with the aim of a strain sensitivity of 10^{-22} (see e.g. Roberston, 2000).

1.3 Types of Detector

1.3.1 Bar Detectors

A simple device for searching for these strains in space is called a Weber bar(Weber, 1968). It consists of a large, solid piece of metal with transducers attached to the middle of it to monitor the oscillations of the bar. The first such device was constructed by Joseph Weber in the 1960s. It consisted of a 1 tonne aluminium bar hung as a pendulum and kept in a vacuum chamber to reduce external noise (Robertson, 2000).

The bar detector (such as the one shown in figure 1.2) can be modeled as two masses joined by a spring. A passing gravitational wave will induce a change in the proper length of the bar and thus the separation of the two masses. The fundamental resonance of the bar will be excited. As the bar will take some time to "ring down", the bar will "remember" the gravitational wave for some time. Hence sensing error can also be reduced through averaging. However, unless the frequency of the gravitational wave is close to the resonant frequency of the bar it will go undetected. Hence these devices are *narrow* band.

The main source of noise in bar detectors is thermal noise. This can be reduced by cooling the bar to close to absolute zero. Research is underway into using the principles of bar detectors to build spherical detectors. These will have many resonances, so will be more broadband. They will also be able to provide additional information such as determining the direction of the incoming wave (V Fafone, 2006).

There is an alternative form of detector that offers the possibility of high sensitives over a broader frequency range. These are called interferometric gravitational wave detectors.

Figure 1.2: The AURIGA bar detector in Italy consists of an aluminium bar cooled to 0.1K. It has a sensitity of less than 3×10^{-9} $Hz^{-1/2}$, but is still far above the required sensitivity of $10^{-22}Hz^{-1/2}$ to detect a gravitational wave. It operates at around 900Hz

1.3.2 Interferometric Gravitational Wave Detectors

A laser interferometric gravitational wave detector in its simplest form is a Michelson interferometer. The perpendicular arms of the detector are well suited to the detection of quadrupolar gravitational radiation (see figure 1.3). The "strain" in space from a gravitational wave propagating perpendicular to the the plane of the interferometer, will result in a differential change in the path lengths of the arms of the interferometer. Due to the quadrupolar nature of the gravity waves, a reduction in the path length in one arm is accompanied by an increase in path length of the other, thus multiplying the sensitivity by a factor of two. A change in intensity pattern at the output of the interferometer will result.

To make as accurate a measurement as possible, the interferometer is "locked" onto a dark interference fringe. This is achieved by sensing any changes in intensity at the interferometer output with a photodiode, and feeding the resulting signal back with suitable phase to a transducer, which is capable of changing the position of one of the interferome-

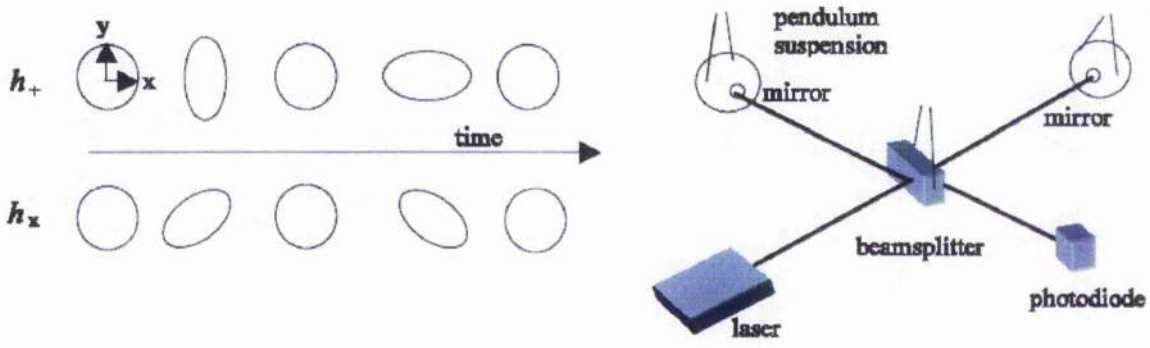

Figure 1.3: The quadrupole nature of gravitational radiation can be seen on the left side of the diagram. If the mirrors of the Michelson Interferometer lie on the ring with the beamsplitter in the middle, the relative lengths of the two arms will change.

ter mirrors (see e.g. Hough, 2005). In this way, a gravitational wave will result in photons "leaking" through one of the arms, and its presence can be uncovered by examining the feedback signal.

To reduce noise in the system, the mirrors (test masses) are suspended as pendula. The arms of the interferometer are also housed in a vacuum chamber. The test masses are usually widely spaced, although there is a limit to how far they can be separated (several km) due to the curvature of the Earth. The expected wavelengths of gravitational radiation place limits on the need for arm lengths more than several km.

Interferometric Gravitational Wave detectors offer the greatest prospect of detecting gravitational waves. There are a number of detectors around the world including: GEO (Germany), VIRGO (Italy), TAMA (Japan) and LIGO (USA) (see figure 1.4) . LIGO and GEO have even begun collecting real scientific data in a number of science runs as they approach their design sensitivity. A great amount of research is being undertaken around the world into the development of next generation gravitational wave detectors,

Figure 1.4: One of the LIGO gravitational wave detectors in Livingston, Louisiana. The other detector is over 3000km away in Richland, Washinginton. The arms of both detector are four km long and are housed in an ultrahigh vacuum system. Using two detectors the detection of a signal can be validated, and the origin can be determined.

with increased sensitivity. This will be achieved by reducing various sources of noise in the detector.

1.4 Sources of Noise

There are a number of sources of noise in interferometric gravitational wave detectors that must be minimized to increase our chances of detecting a gravitational wave and the most important of these will now be discussed (see e.g. Hough and Rowan, 2000):

1.4.1 Seismic Noise

Seismic Noise results from ground motion/vibration as a result of tectonic plate motion/earthquakes, sea waves crashing on the coast, human activity etc. Isolation of motion in the horizontal direction is provided by means of suspending the test masses as

pendulums. As the test masses are pointing towards the center of the Earth, if they are separated by several km, they will be non-parallel because the Earth is curved. Therefore due to coupling of motion between the vertical and horizontal motion, vertical damping is also required. This is provided by a series of springs.

1.4.2 Photoelectron Shot Noise

The induced change in length of the arms of the interferometer results in a small change in the intensity of light observed at the interferometer output. However, there will already be random fluctuations in the intensity of light because the number of photons arriving at the detector, n, are subject to Poisson statistics (a gaussian with standard error $\frac{1}{\sqrt{(n)}}$ where n is very large). The *fractional* precision of a single measurement of the photon arrival rate, in some time τ, is thus given by $\frac{1}{\sqrt{(\overline{n}\tau)}}$. Therefore to ensure these random fluctuations are not of the same order as fluctuations in intensity due to a gravitational wave, this form of loss can be reduced by increasing the number of photons incident at the output of the detector i.e increasing the power of the laser.

1.4.3 Thermal Noise

Thermal noise arises from the thermal motion of the atoms in the test masses and suspension elements which is peaked at the natural resonances. The masses and suspension elements are therefore constructed so that the resonances are far from gravity wave frequencies of interest. However, thermal noise in the *tails* of these resonances can enter the detection band. It is shown in the next chapter that this off resonance thermal noise can be reduced by using materials for the test mass and suspension elements that have a low mechanical loss.

Chapter 2

Thermal Noise

Thermal noise is expected to be a significant source of noise for long baseline gravitational wave detectors. It consists of two components:

1. Thermoelastic Noise - this results from temperature fluctuations in the system
2. Brownian Thermal Noise - results from $\frac{k_B T}{2}$ energy per degree of freedom in a system (where k_B is Boltmann's and T is the temperature of the system). This thermal energy is stored in the translation, vibration and rotation of the atoms in the system. This energy will combine to produce the effect of thermally induced motion of the test mass and suspension modes of the detector, causing a form of displacement noise on the front face of the test mass. Its importance depends on the level of internal friction in the system (mechanical loss), which can be determined via application of the Fluctuation Dissipation Theorem.

2.0.4 Thermoelastic Loss

Thermoelastic loss is associated with the flexing of a thin suspension element. As the element flexes, the side that compresses becomes hotter; the side that expands cools. There is heat flow until a equilibrium is reached, which results in loss. The mechanical

loss associated with thermolelastic damping, which has a frequency dependence ω, is given by equation 2.1 (Nowick and Berry, 1972).

$$\phi_{th}(\omega) = \frac{Y\alpha^2 T}{\rho C}\frac{\omega\tau}{1+\omega\tau^2} \tag{2.1}$$

Where Y is the Young's Modulus, α the thermal coefficient of expansion, ρ is the density, τ is the relaxation time and C is the specific heat per unit volume of the element. The frequency at which this form of loss is at its maximum is given by equation 2.2.

$$f_{circ} = \frac{1}{2\pi\tau} = c \times \frac{\kappa}{\rho C D^2} \tag{2.2}$$

κ is the thermal conductivity. The constant, c, in front of equation 2.2 is a geometrical factor: it is equal to 2.16 in the case of a cylindrical fiber and $\frac{\pi}{2}$ in the case of a ribbon fibre.

2.0.5 Brownian Thermal Noise

In 1827, the botanist Robert Brown was puzzled when he observed the random motion of pollen grains left to float freely on the surface of water. Brown repeated the experiment with particles of dust and in this way was able to rule out that the "jittering" he observed under the microscope was due to pollen particles being 'alive'. However, the origin of the motion remained a mystery, until in 1905 Einstein realized that this motion is a result of the stochastic collisions of water molecules with the pollen grain. He also realized that, due to the viscosity of water, the pollen grains were losing kinetic energy as they moved. He therefore made a connection between a *fluctuation* which excites a system (the irregular impacts between the water particles and the pollen), and a *dissipation* which dissipates energy away from a system (i.e the loss of kinetic energy due to the viscosity of water). This relationship was later developed into something called the

Fluctuation Dissipation Theorem which is a powerful tool used when studying thermal noise.

Fluctuation Dissipation Theorem

The fluctuation dissipation theorem relates the power spectral density S_w of the thermal driving force of a system, to the dissipative (or real) part of the mechanical impedance *Z(w)*:

$$S_F(f) = 4k_bT\Re[Z(w)] \tag{2.3}$$

It can be shown that when the internal modes of the system are modeled as damped-simple harmonic oscillators, with resonant angular frequency ω_0, the displacement thermal noise takes the form of equation 2.4 (e.g. Crooks, 2003).

$$S_x(w) = \frac{4k_BT}{w}\frac{\phi(w)w_0^2}{m[\phi^2(w)w_0^4 + (w_0^2 - w^2)^2]} \tag{2.4}$$

Far below resonance $\omega << \omega_0$, equation 2.4 can be reduced to:

$$S_x(w) \approx \frac{4k_BT\phi(w)w_0^2}{mw(w_0^4\phi(w)^2 + w_0^4)} \approx \frac{4k_BT\phi(w)}{mww_0^2(\phi^2(w) + 1)} \tag{2.5}$$

If we are using a material with a very low mechanical loss, then $\phi^2(w_0) << 1$. Hence:

$$S_x(w) \approx \frac{4k_BT}{mw_0^2}\frac{\phi(w)}{w} \tag{2.6}$$

Equation 2.6 can be used to calculate the level of thermal noise in the detection band. Far above resonance $\omega >> \omega_0$ it can be shown that:

$$S_x(w) \approx \frac{4k_BTw_0^2}{m}\frac{\phi(w)}{\omega^5} \tag{2.7}$$

Therefore, from equation 2.6 and 2.7 it can be seen that there is a significant reduction of thermal displacement spectral density away from resonance when materials with a low mechanical loss factor are used. What about the level of noise at resonance?

From equation 2.4 (where $\omega = \omega_0$):

$$S_x = \frac{4k_BT}{m\omega_0^3}\frac{1}{\phi(\omega_0)} \tag{2.8}$$

Hence there is an *increase* in thermal spectral density at resonance. This is a result of the conservation of energy: the total integrated thermal noise over *all* frequencies must be the same. However, it is the *shape* of the thermal noise spectrum as a function of frequency that is important. By using low loss materials, more of the thermal noise is kept in the resonances of the system, which are arranged so they are far from the frequencies of interest.

Reducing off-resonance thermal noise is much easier than reducing the total thermal noise of the system, which would involve cooling the optics and test masses. Therefore, for good thermal noise performance it is important to choose materials for the detector that have low mechanical loss.

2.1 Silica as a Test Mass Material

Silica (SiO_2) is the current choice of test mass material for Gravitational Wave Detectors (Reid, 2006). Its thermal noise properties are excellent. Silica has a low thermal expansion coefficient ($0.4 \times 10^{-6}\mathrm{K}^{-1}$) and therefore low levels of thermoelastic loss. It has a very low internal dissipation factor: loss measurements better than 10^{-8} have been measured. Its internal dissipation has a frequency dependence. This is beneficial as thermal noise

is expected to be an issue at the lower frequency end of the operating spectrum. The internal loss factor is lower at lower frequencies.

In practical terms, Silica is available in the required sizes to be cut and polished into the test mass mirrors (several 10 kgs). It has a high tensile strength (110 MPa), so silica fibers can be used to suspend silica test masses. Using a setup where the suspension elements and test masses are composed of the same material (monolithic) can also be shown to improve thermal noise performance. A low thermal expansion coefficient is also beneficial as there will be less thermal deformation of the mirror faces when using high powered lasers necessary to reduce shot noise.

This thesis describes a number of measurements made on mechanically polished silica cantilevers. These measurements are then compared to Steve Penn's Empirical Model for losses in fused silica.

2.2 Penn's Empirical Mode

Since the model from Penn et al is discussed in more detail in the following chapter, it will only be mentioned briefly here.

A semi-empirical model has been developed for the mechanical loss in fused silica. It includes dependencies on both surface-to-volume ratio and frequency. It takes the form of (Penn et al, 2005):

$$\phi(f, \frac{V}{S}) = C_1(\frac{V}{S})^{-1} + C_2(\frac{f}{1Hz})^{C_3} + C_4\phi_{th} \tag{2.9}$$

Where V is the volume of the substrate, S is the surface area of the substrate and $C_1..C_4$

are constants chosen depending on the type of silica being studied. ϕ_{th} is a term attributed to thermoelastic loss as discussed previously. The surface loss term $C_1(\frac{V}{S})$ is of particular interest. The mechanisms of loss on the surface of silica are poorly understood. However, some possible sources of surface loss have been speculated:

1. Contaminants absorbed into the surface from the surroundings or from polishing.

2. General or (local) surface roughness.

3. Micro-cracks on the surface of the silica.

The constants used in the model are derived from a fit to many loss measurements taken from various sources. Since these constants are the *best fit coefficients* of equation 3.13 when it is fitted to a data set, they are not quoted with any errors (See Penn et al). This thesis describes measurements taken of suprasil 312. For this silica the constants have the following values:

1. $C_1 = 7.12 \times 10^{-9}$

2. $C_2 = 4.63 \times 10^{-12}$

3. $C_4 \approx 1$

C_3 is associated with the power law exponent in Penn's equation and is found to be approximately 0.813 for silica of this type. The model, however, does not differentiate between silica with different surface conditions. The constants only depend on the type of silica used. The silica samples studied are mechanically polished. It is found that silica with a "pristine" surface has measured losses that lie closer to those suggested by the model. By "pristine" I mean that the factors listed above as possible sources of surface loss are minimized due to careful handling/preparation etc.

2.3 Measuring Mechanical Loss

It has been shown that using material with a low mechanical loss will reduce off-resonance thermal displacement noise. The details of the experimental setup will be outlined later, but the basic principle of measuring mechanical loss in the laboratory is discussed.

The mechanical loss for materials used in gravitational wave detectors is very low, so it is difficult to measure over a broad range of frequencies (see e.g. Reid, 2006). However, near resonance it can be shown that:

$$Q(\omega_0) = \frac{1}{\phi(\omega_0)} \tag{2.10}$$

Where ω_0 is the frequency at resonance of the cantilever being studied. Q is known as the *quality factor* of the material and is equal to the inverse of the mechanical loss at resonance. Hence the mechanical loss of a cantilever can be estimated if its quality factor near resonance can be determined.

To measure the quality factor the resonant modes of a cantilever, which is clamped rigidly at one end, are excited using an electrostatic drive plate. The excitation is then turned off, allowing the modes to decay naturally. The oscillation is monitored by using using a laser to cast a shadow of the cantilever on a split photodiode. In this way the rate of decay of a resonance can be studied using a spectrum analyzer.

The decay will take the form of equation 2.11

$$A(t) = A_0 e^{-\frac{1}{2Q}\phi_{total}(w_0)} = A_0 e^{-\frac{1}{2}\phi_{total}(w_0)w_0 t} \tag{2.11}$$

A_0 is the initial amplitude of the oscillation. Equation 2.11 can be rearranged giving:

$$\ln[A(t)/A_0] = -\frac{w_0 t \phi_{total}(w_0)}{2} \tag{2.12}$$

Hence, by fitting a function to the envelope of the decay, the quality factor at resonance can be found and the mechanical loss follows as its inverse (see figure 2.1).

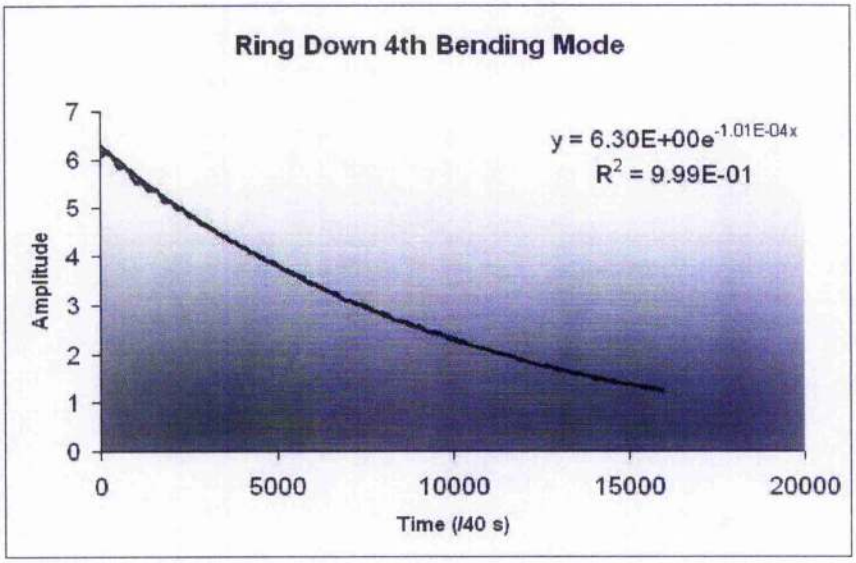

Figure 2.1: This is an example of a ring down of one of the bending modes of a 500 micron thick cantilever. The ring down shows the high quality of data obtained which was typical through most of the results.

To determine the loss of the sample accurately it must be free to move, but also sufficiently isolated from the rest of the world. Other sources of external dissipation must be minimized. These include:

1. Gas Damping - this is reduced by exciting the cantilever in a vacuum tank, with a very low pressure (less than 10^{-5}mb.)

2. Frictional (Slip-stick) damping - dissipation at the point where the suspension element meets the cantilever. This is minimized by first welding the cantilever onto a larger silica block which is then clamped in place.

3. Recoil Damping - this results from energy dissipation from the cantilever into the surrounding structure. This can be reduced in the same way as slip-stick losses, by welding the cantilever onto a larger silica block, or by isolation of suspension point from the rest of the world, for instance by using a pendulum.

Chapter 3

Reducing Mechanical Loss of Mechanically Polished Silica Surfaces through Chemical Etching

3.1 Introduction

In interferometric gravitational wave detectors, the test mass and suspension elements have a very low mechanical loss (high quality factor) in order to reduce off resonance thermal displacement noise (see chapter 2). Fused Silica, which meets both the mechanical and optical requirements, is the current choice of test mass material. Hence the mirrors in the interferometer are fabricated from fused silica test masses. These are mechanically polished and coated with high-reflectivity coatings. It is known that mechanical polishing of silica substrates results in a damaged and contaminated surface layer (Kozlowski et al, 1998). It is of interest to know how deep and how lossy this layer is. This has been studied by etching a mechanically polished cantilever to investigate any correlation between the extent of etching and the measured losses. All sources of mechanical loss, including their magnitude and location with respect to the incident laser beam, must be taken into

consideration to accurately estimate the level of thermal noise in the detection band.

3.2 Background

As mentioned earlier, the semi-empirical model from Penn et al, equation 3.1 decomposes the total loss in fused silica into three sources. There is a term attributed to the frequency dependent bulk loss in fused silica ($C_2(\frac{f}{1Hz})^{C_3}$)(Wiedersich et al, 2000) and also energy dissipated due to heat flow, thermoelastic loss ($C_4\phi_{th}$). The surface loss term ($C_1(\frac{V}{S})$), is of particular interest.

$$\phi(f, \frac{V}{S}) = C_1(\frac{V}{S})^{-1} + C_2(\frac{f}{1Hz})^{C_3} + C_4\phi_{th} \tag{3.1}$$

The model is semi-empirical: the constants (C_1, C_2 and C_4) are fitted from the results obtained from a number of experiments, each with their own error. If samples with a high quality surface (e.g. flame polished or flame pulled) are measured and the conditions of the experiment are favourable, it is possible to produce loss measurements that are lower than the model predicts. This has been seen in Glasgow with measurements of flame drawn ribbon fibres (A.Heptonstall et al, 2006).

However, in this thesis measurements are described for cantilevers that are mechanically polished. Loss measurements obtained for polished silica substrates are generally higher than those obtained from flame polished or flame pulled silica (Penn et al, 2005). This is because the surface of the silica will have been damaged by the abrasive polishing. There is evidence to suggest that the structural surface damage layer is twice as thick as

the abrasive substance used to prepare the samples[1]. For polishing, the typical particle size is 1μm. Therefore the layer, of damage, rather than a very shallow layer, could extend several microns into the silica.

The measured loss of these polished silica cantilevers may be reduced by improving the quality of their surfaces. It is known that a significant increase in the quality factor of silica has been achieved through the use of annealing. One reason for this might be that the surface of the silica is improved (Ageev et al, 2004). It is of interest to discover if a similar reduction is seen in the mechanical loss when the first few microns of the surface are chemically etched away.

[1]Gravity Probe B html: http://einstein.standford.edu/content/topics/pg4.html

3.3 Experimental Setup

It was necessary to calculate the etch rate accurately of a number of etchants: Ammonium Difluoride and Hydrofluoric Acid (buffered and unbuffered). For the work carried out in this section to establish the etch rate of the various chemicals, two surface profiling machines are used: a Veeco optical profiling machine (WYKO NT1100) and a Talysurf contact profiling machine, see figure 3.1.

Figure 3.1: The Talysurf Contact Profiler is shown on the left, the Veeco Optical Profiler is on the right.

The WYKO optical profiler is a non-contact profiler: it uses interferometry to profile a sample surface. It has two operating modes the VSI and PSI.

The PSI (phase shifting interferometry) involves the sequential shifting of the phase of one beam of the interferometer relative to the other beam, which is being reflected from the surface of the sample. Since it is shifted by known amounts, measuring the resulting interference pattern allows details about the surface topography to be extracted (Caber, 1993). This mode is useful for resolving features less than 160 nanometers in size and therefore is appropriate for smooth surfaces e.g. polished and super-polished surfaces.

The VSI mode (vertical shifting interferometry) operates by making incremental movements of a mirror on one of the arms, until a maximum intensity pattern is observed. Hence , by knowing how far the mirror has moved to achieve maximum intensity, the size of the corresponding surface feature can be determined (Zecchino, Novak and Schmit, 2006). This is done for each point on the surface. The VSI mode is used to profile features less than 2mm and was used for the measurements taken later in this thesis.

The WYKO comprises a microscope and an interferometer, so it can be very useful in providing three dimensional images of surfaces at various magnifications such as those shown in figure 3.2

The Talysurf profiler is a contact profiler: a finely tipped diamond stylus (2μm in radius) transverses the surface. Since it moves with constant velocity, the diamond tip can be tracked along the x-axis. The tip's motion in the vertical plane is sensed by a coil-magnet transducer. Hence it can build up a profile of surface topography, but only in two dimensions (Bennet and Dancy, 1981).

Both machines can provide a wealth of surface statistics. One statistic that will be used later is the mean peak-to-valley height R_z. In three dimensions, this is typically calculated as the average maximum profile of the ten greatest peak-to-valley separations in the evaluation area.

The etch rate of three common corrosive chemicals was determined: Ammonium Difluoride, Hydrofluoric Acid (HF) and Buffered Hydrofluoric Acid (Hydrofluoric and Ammonium Difluoride). A silica slide (Suprasil 3) was clamped and partially immersed in each of the chemicals. After a given time, more of the chemical was added to the beaker, so that more of the slide is immersed in the chemical. This is done repeatedly. As each

part of the slide spends more time in solution than the part above it, this has the effect of producing a series of steps across the surface of the silica.

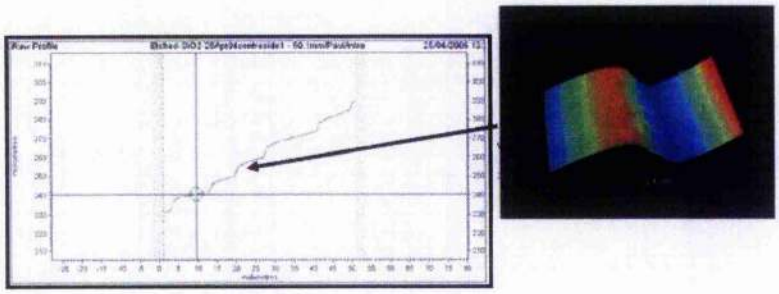

Figure 3.2: Here we see a step on the Talysurf contact profiler (left) and the corresponding step as seen on Veeco optical profiler(right).

The steps can be seen clearly on both profiling machines in figure 3.2. By using the profiling machines to measure the size of the steps it is possible to calculate the etch rate.

Since the interval after which more chemical is added is approximately the same, the steps are expected to be approximately the same size. Therefore a mean value of the step size and a standard error in these results can be calculated. This gives a more accurate etch rate than in the case of a single measurement. Further, all the steps are formed under approximately the same conditions, which is of benefit as the etch rate is sensitive to a number of factors such as concentration and temperature (see Appendix A).

The procedure for both machines is outlined in the figure 3.3. The steps can be seen on the raw data profile from the talysurf contact profiler (3.3a). First, the computer is used to highlight the step of interest. The bottom of the step is "flattened": the computer removes the incline from this part of the sample (3.3b and 3.3e). This makes the bottom of the step the reference point. This was done using the software included with both of the machines. Next, in the case of the Talysurf, we can zoom into the step and read the

height off the Y-axis (3.3c). For the optical profiler, since the bottom of the step has been flattened, the step height is equivalent to the R_z statistic described earlier (3.3f).

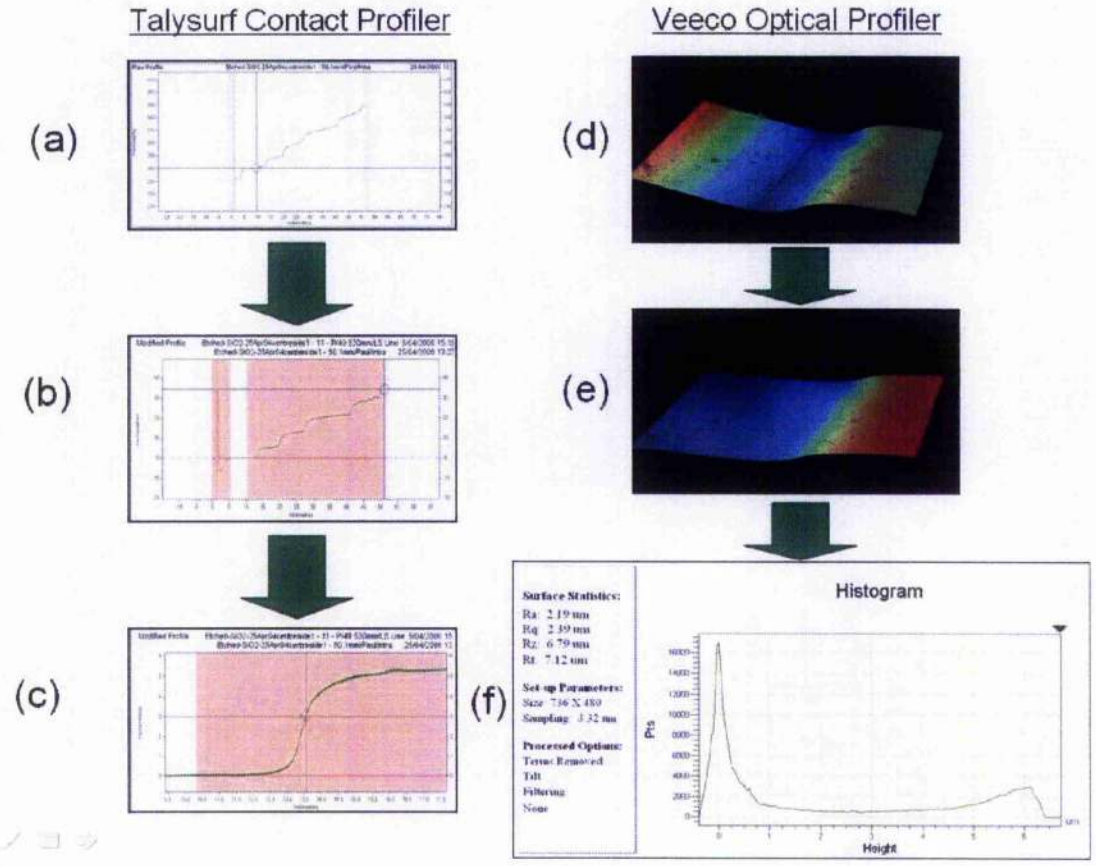

Figure 3.3: The flow chart outlines the procedure to measure step size for each profiling machine.

There are a number of sources of error. There is the error in the length of time after which more of the etchant is added to the beaker. In the case of the HF, more solution was added every fifteen minutes. However, as a result of human error, this was taken to be fifteen minutes $\pm$ 30 seconds. Further, there is the limit to the accuracy of the talysurf profiling machine. It is difficult to see exactly where the transition between the bottom and top of the step ends (1.3c) because the limit of the vertical resolution of the machine is being approached. To isolate the machine from background noise, it was placed on a heavy granite slab. However, the machine was still not performing optimally. Therefore the error in the resolution of the talysurf was taken to be plus or minus 0.1 micron. The optical profiler, on the other hand, has a vertical resolution of less than 1nm (for VSI), so the error in its accuracy was taken to be negligible in comparison to other sources of error. The size of the steps should be equal since they correspond to approximately the same length of time in solution. However, there is a spread of values for the step heights, allowing a standard error to be calculated. All of these errors are added together in quadrature to produce a final error for each of the etch rates.

3.3.1 Results

An example of how the etch rate of HF is calculated, including the error, is outlined. In table 3.1 there is a list of the steps from the HF and their corresponding size in microns measured by the Talysurf contact profiler.

Step	Size (microns)
1	7.6
2	5.2
3	6.62
4	5.1
5	6.1
6	6.3
7	5.8
8	6.5
9	6.4
10	6.1
	$\bar{x}=\frac{\sum_n}{10}$=6.17
	Standard Error = $\frac{\sigma}{\sqrt{10}}$=0.23

Table 3.1: A list of step sizes in microns for the five steps on either side of the Suprasil 3 slide, with the mean step size and the standard error quoted. The slide was etched in Hydrofluoric Acid.

Using the data above, the etch rate of HF is calculated as follows. The etch rate in one hour = $\bar{x} \times 4$ = 6.17 ×4 = 24.69 micron/hr. Hence the etch rate in one second = $\frac{24.69}{3600}$ = 0.0069 micron/s. There is an error of plus or minus thirty seconds, after which more solution is added. This corresponds to 0.0069 × 30 = 0.21 micron. There is also an error of $\pm\frac{1}{10}$ micron, the sensitivity of the Talysurf. Finally, all these errors are added together in quadrature. This gives: error=$\sqrt{0.21^2 + 0.1^2 + 0.228^2}$ = 0.32 micron.

Etchant	Ammonium Difluoride	Hydrofluoric Acid (40%)	Buffered HF (40%)
Etch rate (microns per hour)	4.89± 0.39	24.69± 0.32	9.87± 0.20

Table 3.2: The etch rates of Ammonium Difluoride (40g added to 200ml water), Hydrofluoric Acid and Buffered Hydrofluoric Acid. All measurements were carried out at room temperature.

Hence the etch rate of HF= **24.69 ± 0.32 microns/hr.** A similar calculation was carried out for the other etchants. The results are in table 3.2

3.4 Comparison of Transition Line between HF and Buffered HF

A comparison of the transition line (that is the boundary between each of the steps as seen in figure 1.2) is made for for HF and Buffered HF, using the Veeco optical profiling machine. With HF, not only is there etching of the silica that is immersed in the liquid but also, via evaporation, etching of the silica above the surface of the liquid. Ammonium Difluoride is added to the hydrofluoric acid to significantly reduce this effect. One reason for this could be that making the solution buffered helps maintain a constant pH at the surface where evaporation occurs, thus maintaining a constant etch rate. This is important in the context of our experiment. The cantilever (suprasil 3 slide) is welded onto a larger silica mass to reduce clamping losses. If the slide is immersed in etchant to remove its surface layer, any etching above the surface of the liquid could lead to slight etching at the weld. Therefore, to prevent changes in the quality of the weld, Buffered HF is the chemical chosen to etch the cantilevers used to study mechanical loss.

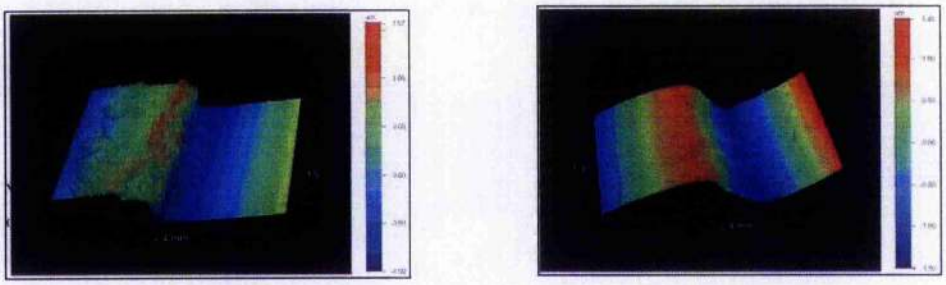

Figure 3.4: The transition across each step for buffered HF (left) and HF (right)

Figure 3.4 illustrates the differences between HF when it is buffered and unbuffered. On the left the HF is unbuffered and there is a smooth but continuous transition across each step. However, in the case of the buffered HF, the change between each step is comparably very abrupt.

3.5 Comparison between Contact and Non-contact Measurements for Etch Rate

It is known that optical and contact profilers can sometimes disagree (Poon and Bhushan, 1995), so it is of interest to compare the results obtained when both machines measure the same sample. For a slide etched in Hydrofluoric Acid, the height of the steps across its surface was measured using both the WYKO optical profiler and the Talysurf contact Profiler.

Step	Size optical profiler (microns)	size contact profiler (microns)
1	7.6	6.90
2	5.2	5.65
3	6.62	6.16
4	5.1	5.89
5	6.1	7.17
6	6.3	5.20
7	5.8	5.78
8	6.5	5.68
9	6.4	4.63
10	6.1	6.36
	$\bar{x}=\frac{\sum_n}{10}=6.17$	$\bar{x}=\frac{\sum_n}{10}=5.94$
	Standard Error $=\frac{\sigma}{\sqrt{10}}=0.23$	Standard Error $=\frac{\sigma}{\sqrt{10}}=0.24$

Table 3.3: Comparison of step size as seen by the optical and contact profiler. Each step corresponds to fifteen minutes in Hydrofluoric Acid

The steps are compared in table 3.3. The mean step heights do agree within error. The etch rate for HF is = **24.69 ± 0.91 /hr** and **23.76 ± 0.96 /hr** for the Talysurf and Optical Profilers respectively.

3.6 Initial Setup

In this section, our efforts to measure the loss as a function of etch depth for a cantilever etched in Buffered HF, welded onto a silica block and fixed in a steel clamp are discussed. The mechanical loss results obtained from this initial set-up are over a magnitude higher than the predictions of the empirical model.

A cantilever (polished suprasil 3 slide) of dimensions 75mm × 12.5mm × 0.5mm was welded onto a larger block of silica dimensions 20mm × 20mm × 20mm see figure 3.6. Welding the cantilever onto a thicker block and then clamping this block in place is intended to reduce "stick-slip" losses associated with the cantilever flexing and grinding in the clamp (T.J. Quinn et al, 1995).

As surface loss was of interest, thin cantilevers were chosen so that the total loss was less likely to be dominated by bulk losses in the silica. A thin cantilever also makes the silica welding more practical. The silica should be hot enough to flow so that the join between the cantilever and larger block is seamless. In reality, due to the high melting point of silica (1723 °C), it is a difficult process. It is very hard to distribute the heat evenly across both surfaces. It can take significant time to produce a satisfactory weld. Overheating the silica can increase the likelihood of producing silica vapour which would be deposited on the cantilever as dust. This will contribute to the surface loss and potentially contribute to the experiment. This will be discussed later.

This system is placed in a vacuum tank (see figure 3.5), the pressure of which is no more than 5×10^{-5} mb. It can be shown that this pressure ensures that the measured loss is not limited by gas damping (S.M. Twyford, 1998).

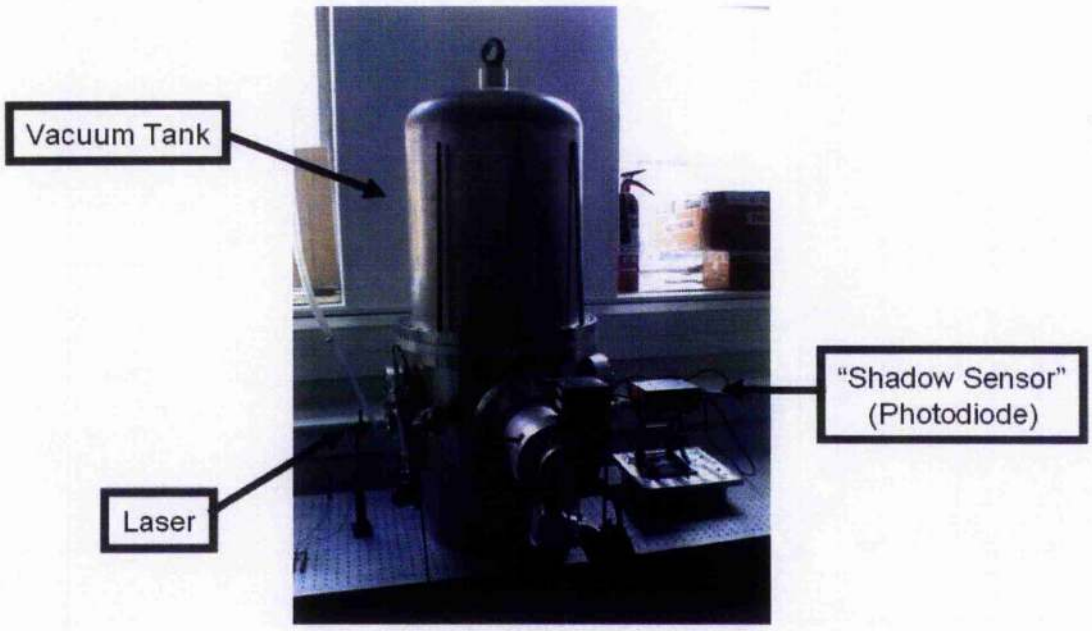

Figure 3.5: The setup used to measure the Q of the etched cantilevers

An electrostatic plate was used to excite each of the modes of the cantilever in turn. A laser shone on the cantilever casts a shadow that falls on a photodiode external to the tank. The motion of the shadow as the cantilever oscillates is recorded. When the electrostatic drive is switched off, these modes are allowed to decay, and from the rate at which they decay their quality factor can be determined (see chapter 2).

First the mechanical loss factor of the first four bending modes of the unetched cantilever are measured. Following this, the slide was held in buffered HF approximately 0.4 cm below the weld point. This was to ensure that etching did not occur near the weld.

Figure 3.6: The suprasil 3 slide welded onto a larger silica mass

In the first instance, the slide was suspended in buffered HF for approximately six minutes (removing a 1 micron surface layer). The quality factors of the bending modes were remeasured. This was repeated until the slide had spent a total of 72 minutes in solution, therefore removing a total of 12 microns from the cantilever surfaces.

3.6.1 Results

From considering the data shown in figures 3.7 and 3.8, there appears little correlation between the measured cantilever losses and the time the cantilever spent etching in the solution. Where error bars are not present, they are too small to be visible on the graph. Due to the high quality of data obtained many of the results presented have standard errors two orders of magnitude smaller than the average values obtained. All important results will have standard errors quoted in tables later.

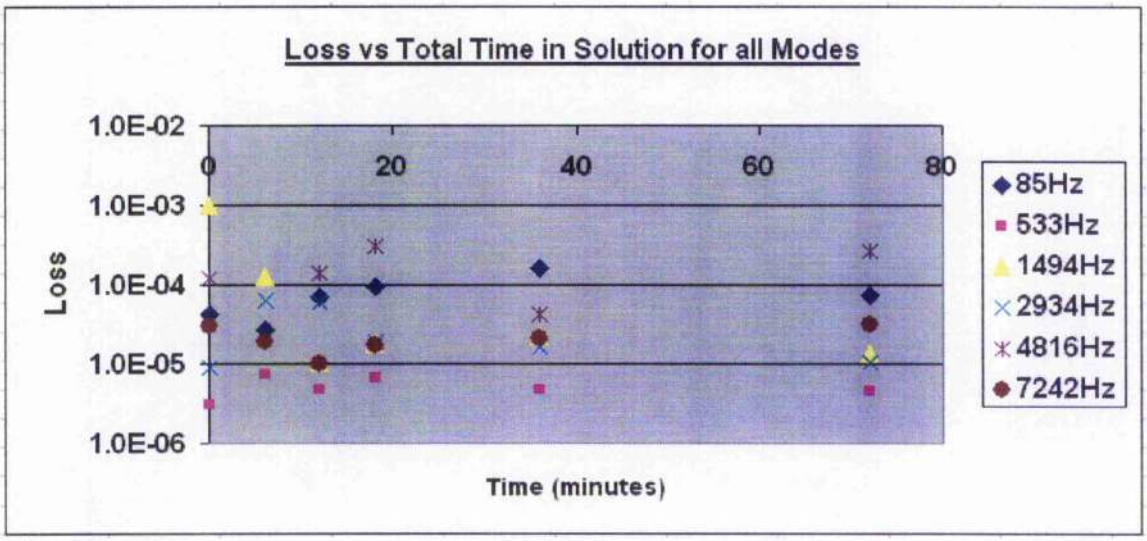

Figure 3.7: A plot of loss against total time in solution for all modes demonstrates that there is no obvious correlation between the etching of the cantilever and the measured losses.

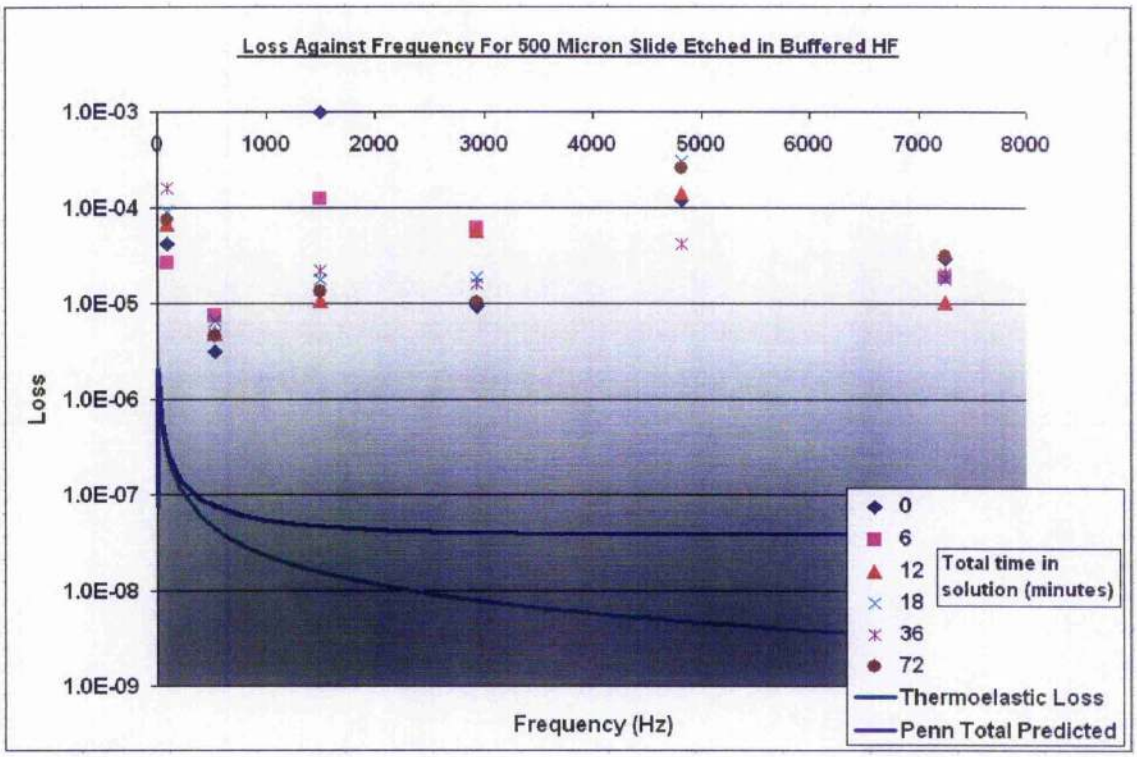

Figure 3.8: The first set of loss results from the 500 micron thick cantilever etched in buffered HF. There is no obvious relationship between the measured loss and the length of time the cantilever spends in solution.

In figure 3.8 two theoretical curves have been included: the thermoelastic curve and the total loss predicted by the empirical model (see equation 3.1). When a comparison is made, the measurements are found to be almost two orders of magnitude higher than the theoretical curves. This suggests that the setup is dominated by some other form of loss that is not intrinsic to the sample itself. This is most likely clamping/recoil loss. Therefore, a new method for measuring the loss of these cantilevers of this size was used: they were welded onto a larger, suspended silica block.

3.7 Optimized Setup

It was believed that the dominant source of loss, in the case of the cantilever being clamped, was energy dissipation in the clamp and clamping structure. By welding the cantilever onto a larger block (in this case a cylindrical test mass) and suspending this block as a pendulum, less energy is likely to be coupled away from system, see figure 3.9. There are a number of reasons why this is the case.

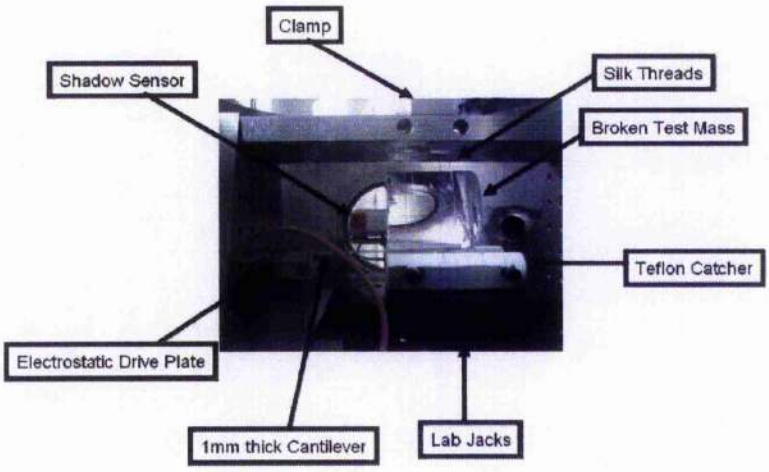

Figure 3.9: A picture of the new suspension in the vacuum tank

In the first setup, the cantilever was welded onto a larger silica block which was fixed rigidly in a steel clamp. There is friction between the steel clamp and silica block. When the cantilever is oscillating, any grinding in the clamp will thus lead to energy dissipation. In the case of the new setup, however, the clamp is monolithic: the silica cantilever is directly welded to a larger silica test mass. Therefore this kind of clamping loss is effectively eliminated.

3.7.1 The System as a Pendulum

By suspending the test mass as a pendulum it is isolated from its surroundings. It is an example of a damped driven harmonic oscillator of the form (Pain, 2000):

$$m\ddot{x} + b\dot{x} + kx = F_0 \cos wt. \tag{3.2}$$

Where m is the mass of the oscillator, k is the spring constant, b is a constant and x is the displacement of the oscillator from equilibrium. The right hand side of the equation is the sinusoidal driving force. From the theory of differential equations, this equation has a solution composed of two parts,

$$x(t) = x_D(t) + \frac{F_0 \cos(\omega - \delta)}{m\sqrt{(\omega^2 - \omega_R^2)^2 + 4\beta^2(\omega_1)^2}}. \tag{3.3}$$

Where $\beta = \frac{b}{2m}$ and $\omega_1^2 = \omega_0 - \beta^2.\omega_0 = \frac{k}{m}$ and ω_R is the *resonant frequency* and is given by $\omega_R = \sqrt{\omega_0^2 - 2\beta^2}$. The phase satisfies $\tan\delta = \frac{2\beta\omega}{\omega_0^2 - \omega^2}$. $x_D(t)$ is the *transient* part of the solution. It depends on the initial conditions of the system, but in any case as it is some function multiplied by the term $\exp^{-\beta t}$ it decays quickly. In the long run (large t) the following *steady state solution* persists:

$$x(t) = A\cos(w_1 + \beta). \tag{3.4}$$

This solution has the frequency of the driving force, i.e. provided by the electrostatic drive plate. The amplitude of this oscillation is given by:

$$A_s(\omega) = \frac{F_0}{m\sqrt{(\omega^2 - \omega_1^2)^2 + (4\beta(\omega_1)^2)}} \tag{3.5}$$

Where the damping β is taken to be fixed and the driving frequency ω as variable. Hence by looking at this equation, the highest amplitude of the system will result when the

driving frequency is the same as the resonance of the pendulum. This would occur if the cantilever was excited at around 2IIz (this frequency was observed from the spectrum analyzer to have a relatively large amplitude with respect to the cantilever's resonant motion) and corresponds to the greatest energy dissipation into the surrounding structure. As long as the frequencies of consideration are far from the pendulum resonance, the system is effectively isolated from the rest of the world.

This could explain later why it is difficult to get an accurate measurement of the fundamental mode. This mode has the lowest frequency and is therefore closer to the resonance of the pendulum. Figure 3.10 shows the shape of the amplitude curve as a function of frequency.

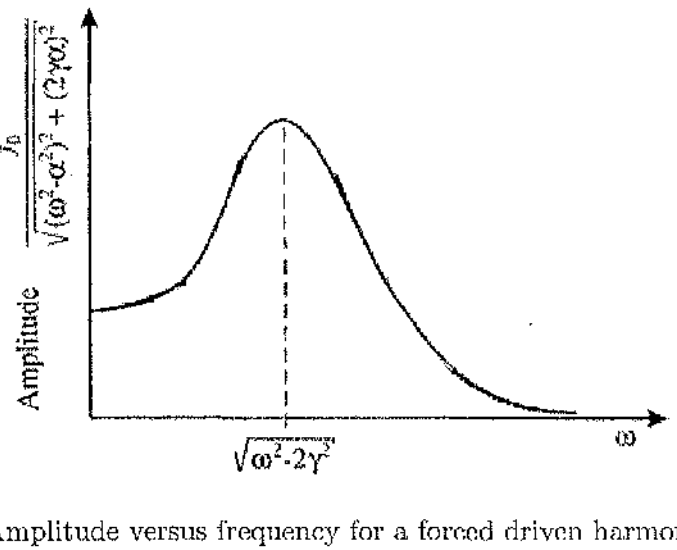

Figure 3.10: Amplitude versus frequency for a forced driven harmonic oscillator.

3.7.2 The System as Two Coupled Oscillators

This system is an example of two coupled oscillators as shown in figure 3.11.

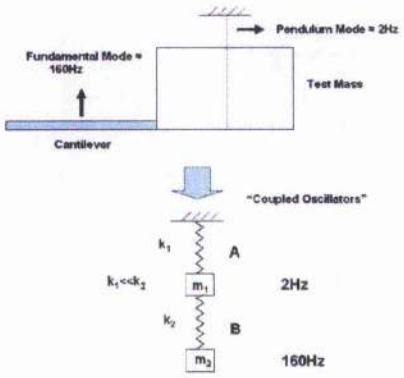

Figure 3.11: The system can be modeled as two coupled oscillators. It is necessary to minimize A, the magnitude of the oscillation associated with the upper spring, because this allows the possibility of dissipation of energy into the surroundings.

The equations of motion for the system are:

$$-k_1 x_1 + k_2(x_2 - x_1) = m_1 \ddot{x}_1 \tag{3.6}$$

$$-k_2(x_2 - x_1) - k_1 x_1 = m_2 \ddot{x}_2 \tag{3.7}$$

Where k_1 and k_2 are the spring constants of the upper and lower spring and m_1 and m_2 are the masses of the attached oscillators as shown in figure 3.11. Re-arranging gives:

$$m_2 \ddot{x}_2 + k_2(x_2 - x_1) + (k_1 x_1) = 0$$

$$m_1 \ddot{x}_1 - k_2(x_2 - x_1) + (k_1 x_1) = 0$$

Writing in standard form:

$$\ddot{x_2} - \frac{k_2}{m_2}x_2 + \frac{k_1 - k_2}{m_2}x_1 = 0$$
$$\ddot{x_1} - \frac{k_2}{m_1}x_2 + \frac{k_1 + k_2}{m_2}x_1 = 0$$

We can write $w_2^2 = \frac{k_2}{m_2}$ and $w_1^2 = \frac{k_1+k_2}{m_1}x_1$. These are known as the first and second partial frequencies associated with both of the springs. w_1 is the frequency of the cantilever (were it oscillating separately) and w_2 is the frequency of the pendulum. This produces a pair of differential equations:

$$\ddot{x_2} + w_2^2 x_2 + \frac{k_1 - k_2}{m_2}x_1 = 0 \tag{3.8}$$
$$\ddot{x_1} - \frac{k_2}{m_1}x_2 + w_1^2 x_1 = 0 \tag{3.9}$$

These equations have a well-known solution in the form:

$$x_1 = A\cos(wt + \phi) \tag{3.10}$$
$$x_2 = B\cos(wt + \phi) \tag{3.11}$$

Where A and B are constants and ω is the frequency of the coupled system. Equation 3.10 can be substituted into the differential equations giving,

$$-w^2 B + w_2^2 B + \frac{k_1 - k_2}{m_2}A = 0$$
$$-w^2 A + w_1 A - \frac{k_2}{m_1}B + w_1^2 A = 0$$

This leads to:

$$\begin{aligned}(w_2^2 - w^2)B &= \frac{k_2 - k_1}{m_2}A \\ (w_1^2 - w^2)A &= \frac{k_2}{m_1}B\end{aligned}$$

Finally, by dividing these two equations and substituting for w_1 and w_2 we find:

$$\frac{A}{B} = \frac{m_2}{m_1}\frac{w_2^2}{w_1^2 - w^2} \tag{3.12}$$

To minimize the energy dissipated from the system, the amplitude of the oscillation, A, must be made small. Since term $\frac{w_2^2}{w_1^2 - w^2}$ is a slowly varying function of m_1 and m_2 (Khusnutdinova and Pelinonsky, 2002), this can be made arbitrarily small by ensuring that m_2, the mass of our test mass, is large in comparison to the mass of our cantilever, m_1. By making the test mass large compared to the cantilever, the recoil of the test mass when the cantilever is excited is reduced and therefore less energy is dissipated away from the system.

Further experimenting was carried out on this system in order to optimize the measured losses. Such questions were considered as, what is the optimum way of suspending the test mass? Does the loss measured depend on the condition or quality of the test mass?

3.8 Results

3.8.1 1mm Slide

Experiments were carried out on a 1mm thick slide (75mm × 13mm × 1mm) welded to an old cylindrical test mass (diameter 65mm, length 70mm).

When searching for a test mass to experiment with, a test mass was found with a piece broken from it. Out of curiosity it was decided to investigate how the measured loss of our cantilever varied depending on the "condition" of this test mass. Three cases were examined: the broken piece sellotaped in place, the broken piece completely removed and finally, the broken piece bonded precisely in place using Hydroxide Catalysis bonding. Each of these cases is considered in turn.

First, the broken piece was taped in place using sellotape. In addition to taping the piece in place, the effect of changing the suspension of the test mass was investigated. The losses of the cantilever were measured when the test mass was suspended on two silk threads, one silk thread, and finally with no suspension. The lowest losses were obtained when the test mass was hung on a single silk thread. These results, including the standard errors, are summarized in table 3.4.

Mode	Suspended On Two Silk Threads	No Pendulum (Sitting On Teflon Catcher)	Suspended On Single Silk Thread
Fundamental 157Hz	$(5.95 \pm 0.016) \times 10^{-5}$	$(8.40 \pm 0.05) \times 10^{-4}$	$\mathbf{(2.748 \pm 0.004)} \times 10^{-5}$
2nd 961Hz	$(1.20 \pm 0.008) \times 10^{-4}$	$(1.13 \pm 0.05) \times 10^{-4}$	$(9.79 \pm 0.05) \times 10^{-5}$
3rd 2677Hz	$(8.90 \pm 0.31) \times 10^{-5}$	$(1.19 \pm 0.05) \times 10^{-4}$	$(1.14 \pm 0.01) \times 10^{-4}$
4th 5215Hz	Not Measured	Not Measured	$(2.90 \pm 0.08) \times 10^{-5}$
5th 8561Hz	Not Measured	Not Measured	$(1.086 \pm 0.009) \times 10^{-5}$

Table 3.4: The set of results with the broken piece taped back onto test mass.

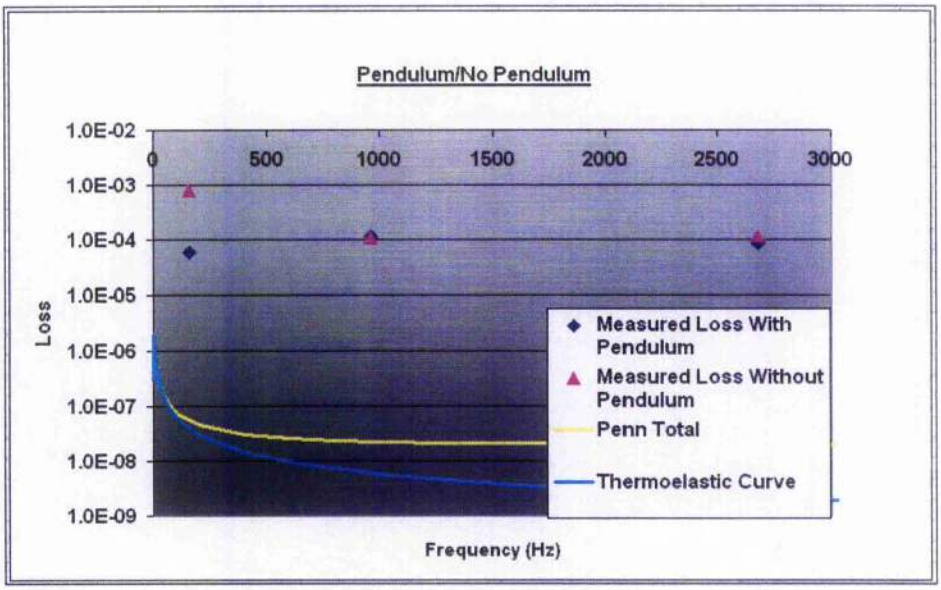

Figure 3.12: A comparison of the measured losses of the modes when the test mass is hung on a pendulum and when it is just sitting on the Teflon Catcher. For the fundamental mode, there is a clear improvement when the test mass is suspended as a pendulum.

From figure 3.12 it can be seen that the results for the 1mm thick slide are still several orders of magnitude higher than predicted by Penn's model.

In the next setup the broken piece was completely removed. All of the modes showed a large increase in quality factor. This suggests that the sellotape was a dominant source of loss in the previous setup. Further experimenting was undertaken on different configurations of the suspension. A double silk loop was used again but this time the clamp was modified so the loops were closer together (from 10 cm separation, to 1.5 cm) around the center of mass of the system (which is approximately the center of the test mass). Moving the loops closer together was found to be an improvement but still not as good as the case of a single loop.

As the lowest losses were obtained with a single loop, this loop was made as short as

Mode	Suspended On One Thread (5cm)	Double Loop 1.5cm Apart	Suspended On One Thread (1.5cm)
Fundamental 157Hz	$(4.26 \pm 0.04) \times 10^{-6}$	$(8.26 \pm 0.03) \times 10^{-6}$	$(1.99 \pm 0.2) \times 10^{-6}$
2nd 961Hz	$(5.49 \pm 0.008) \times 10^{-6}$	$(5.615 \pm 0.008) \times 10^{-6}$	$(5.33 \pm 0.09) \times 10^{-6}$
3rd 2677Hz	$(7.119 \pm 0.09) \times 10^{-6}$	$(5.152 \pm 0.009) \times 10^{-6}$	$(6.47 \pm 0.2) \times 10^{-6}$
4th 5215Hz	$(6.511 \pm 0.008) \times 10^{-6}$	$(6.56 \pm 0.01) \times 10^{-6}$	$(6.28 \pm 0.04) \times 10^{-6}$
5th 8561Hz	Not Measured	Not Measured	Not Measured

Table 3.5: The set of results with the broken piece removed from test mass- all of the modes show decreased loss over the case where the broken piece was taped in place.

possible to see if changing the length of the pendulum reduced the measured loss. This was achieved by moving the clamp from the top of the frame to the underside as shown in figure 3.13. The test mass was raised with a lab jack and a thin piece of teflon placed between the test mass and the clamp to form a space. The thread was put under tension, near to breaking stress, prior to clamping. The teflon piece was removed and then the lab jack was lowered. Hence the suspension length was minimized, as the silk thread was drawn out minimally by the weight of the test mass. This result produced the lowest measured loss as seen in table 3.5.

Figure 3.13: The test mass suspended on a double loop (left). The clamp was moved to the underside of the frame, in order to make the suspension as short as possible for the single loop (right).

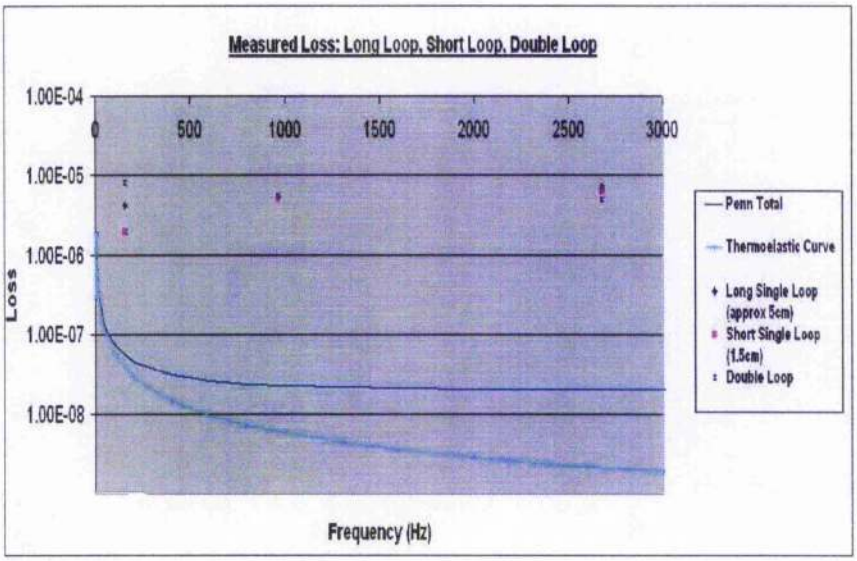

Figure 3.14: For the fundamental mode, the short silk suspension clearly gives the lowest measured loss. The other modes agree within error for the long/short thread. The double loop is the worse for every mode.

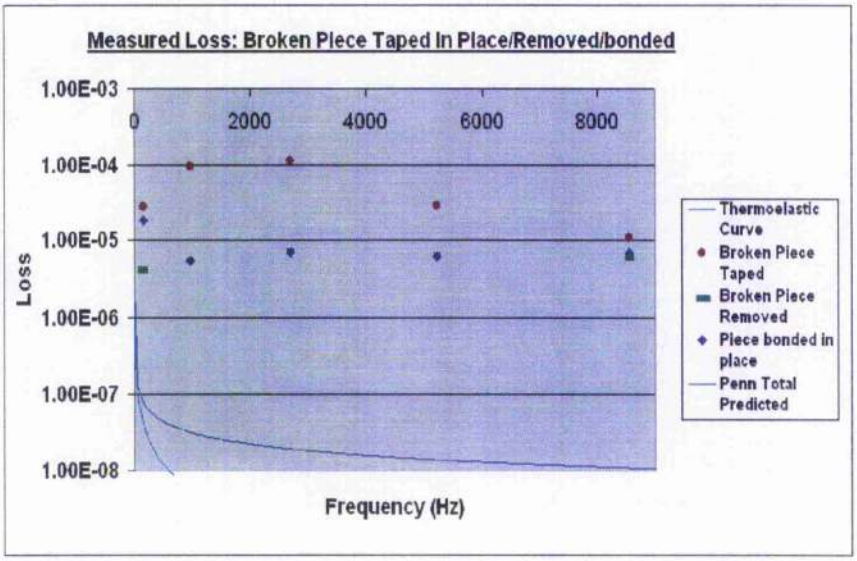

Figure 3.15: The measured losses when the broken piece is taped in place, removed and bonded using hydroxide catalysis bonding. Where the green points are not visible, they lie behind the blue ones.

Mode	Broken Piece Bonded In Place	Piece Removed
Fundamental 157Hz	$(1.83 \pm 0.02) \times 10^{-5}$	$(1.99 \pm 0.2) \times 10^{-6}$
2nd 961Hz	$(5.49 \pm 0.03) \times 10^{-6}$	$(5.33 \pm 0.09) \times 10^{-6}$
3rd 2677Hz	$(6.81 \pm 0.03) \times 10^{-6}$	$(6.47 \pm 0.2) \times 10^{-6}$
4th 5215Hz	$(6.24 \pm 0.05) \times 10^{-6}$	$(6.28 \pm 0.04) \times 10^{-6}$
5th 8561H	$(6.91 \pm 0.06) \times 10^{-6}$	Not Measured

Table 3.6: A lower loss is obtained when the piece is removed over the case where it is bonded in place(The test mass was suspended from one short silk thread in both cases).

Finally, the system was measured when the broken piece was bonded in place using Hydroxode-Catalysis bonding. We used 15ul of KOH solution, of concentration 0.1 mol/l. The results for this, while still an improvement over the sellotaped case, were not better than the case of the piece being completely removed see figure 3.15

It is interesting to ask why lower losses are measured with one silk thread rather than two. One reason could be that one loop has less surface contact with the test mass. Friction between the thread and the test mass will result in loss. Also, a single loop will be in contact only at the center of mass of the system, the place of minimum motion, resulting in less friction. Further, with one loop the quantity of silk used is less than in the case of two loops therefore less energy is dissipated away through the thread.

In addition to measuring lower losses with a single short silk thread, it was also found to be more practical to suspend the test mass in this way. The shorter suspension system was observed to be more stable, tending not to oscillate as much about its center of mass. It is a real problem with the longer suspension that if the system is perturbed in someway (i.e. by banging of a door, knocking bench etc) the rocking mode can be excited to a high level, overloading the lock-in amplifier and making measurements difficult.

In all cases, however, the fundamental and the second mode were the most sensitive

modes to changes in the test mass and suspension. This was particularly true of the fundamental mode. Therefore, it is possible that these modes are suspension limited. One reason for this might be because they are closest to the resonance of the pendulum (see previous section). No conclusions about the sample were reached when looking at these modes.

After some experimenting, it was found that the optimal arrangement was to have the test mass suspended on a short, single silk thread. Not only because for all the modes (particularly the fundamental mode and the 2nd mode) the lowest losses were measured but the setup was also more stable with this configuration.

3.8.2 500 Micron Thick Slide

A 500 micron (75mm × 13mm × 0.5mm) thick cantilever was welded to a new pristine test mass (diameter 65 mm, length 70mm). The test mass was again suspended from a short, single silk thread.

From looking at figure 3.16, the conclusions drawn earlier were correct: cantilevers of this size when measured using the old clamping system (silica welded to large block, in steel clamp) are dominated by clamping losses. The new measurements are far closer to those predicted by the empirical model. An obvious correlation between loss and etching was not observed previously, because the measured losses appeared to be completely dominated by clamping loss.

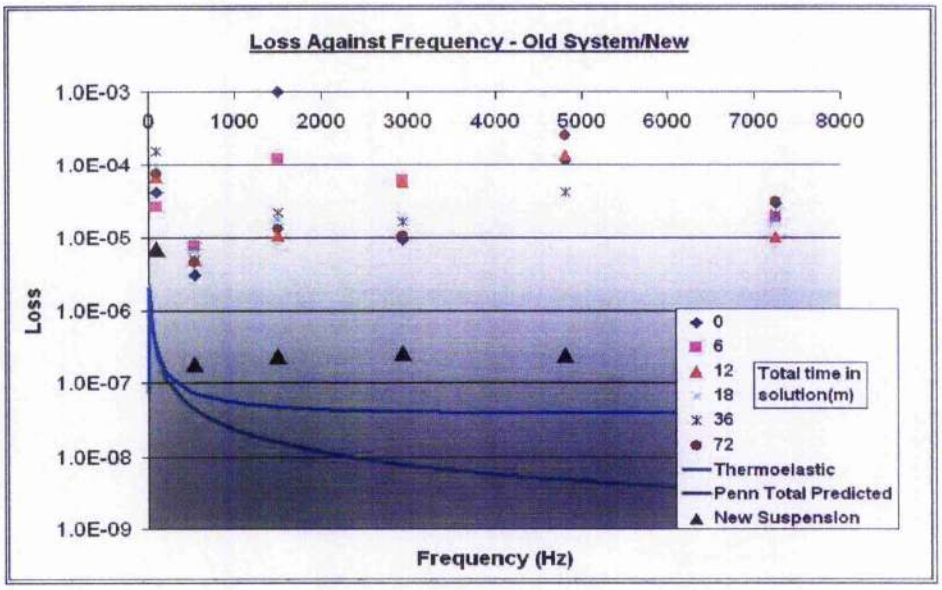

Figure 3.16: The initial results from the old setup (silica cantilever welded to a block and fixed in a clamp) have a far higher loss than the new setup (silica cantilever welded onto a test mass and suspended as a pendulum).

The etching of this 500 micron thick cantilever was repeated as before. This time, a two micron layer was etched from the surface. These results are in table 3.7 and are plotted in figure 3.17

Mode	Unetched Cantilever	Three Minutes Total	Six Minutes Total	Twelve Minutes Total
1st	$(6.8 \pm 0.2) \times 10^{-6}$	$(4.41 \pm 0.08) \times 10^{-6}$	$(4.54 \pm 0.1) \times 10^{-6}$	$(1.71 \pm 0.02) \times 10^{-7}$
2nd	$(1.81 \pm 0.01) \times 10^{-7}$	$(1.86 \pm 0.07) \times 10^{-7}$	$(1.86 \pm 0.04) \times 10^{-7}$	$(1.90 \pm 0.07) \times 10^{-6}$
3rd	$(2.31 \pm 0.02) \times 10^{-7}$	$(1.54 \pm 0.03) \times 10^{-7}$	$(1.61 \pm 0.02) \times 10^{-7}$	$(1.79 \pm 0.02) \times 10^{-7}$
4th	$(2.570 \pm 0.002) \times 10^{-7}$	$(1.47 \pm 0.02) \times 10^{-7}$	$(1.61 \pm 0.03) \times 10^{-7}$	$(1.65 \pm 0.001) \times 10^{-6}$
5th	$(2.39 \pm 0.04) \times 10^{-7}$	$(1.490 \pm 0.003) \times 10^{-7}$	$(1.60 \pm 0.07) \times 10^{-6}$	$(1.61 \pm 0.07) \times 10^{-6}$

Table 3.7: The loss results of the cantilever etched in buffered HF. The greatest reduction in loss is after the first 0.5 micron layer is taken off the surface.

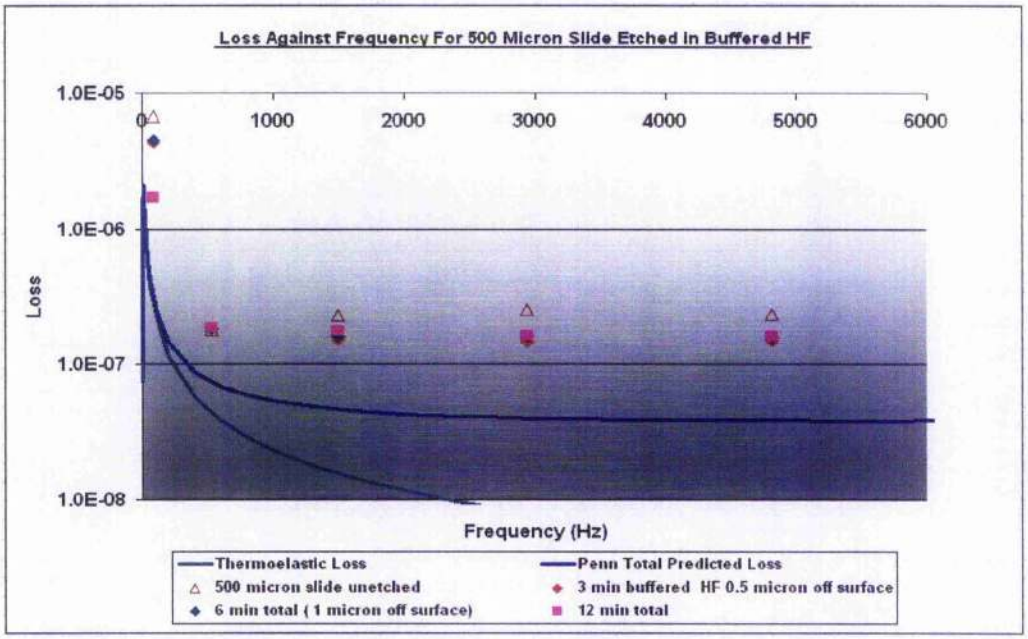

Figure 3.17: The measured loss as a function of frequency taken from the etched cantilever.

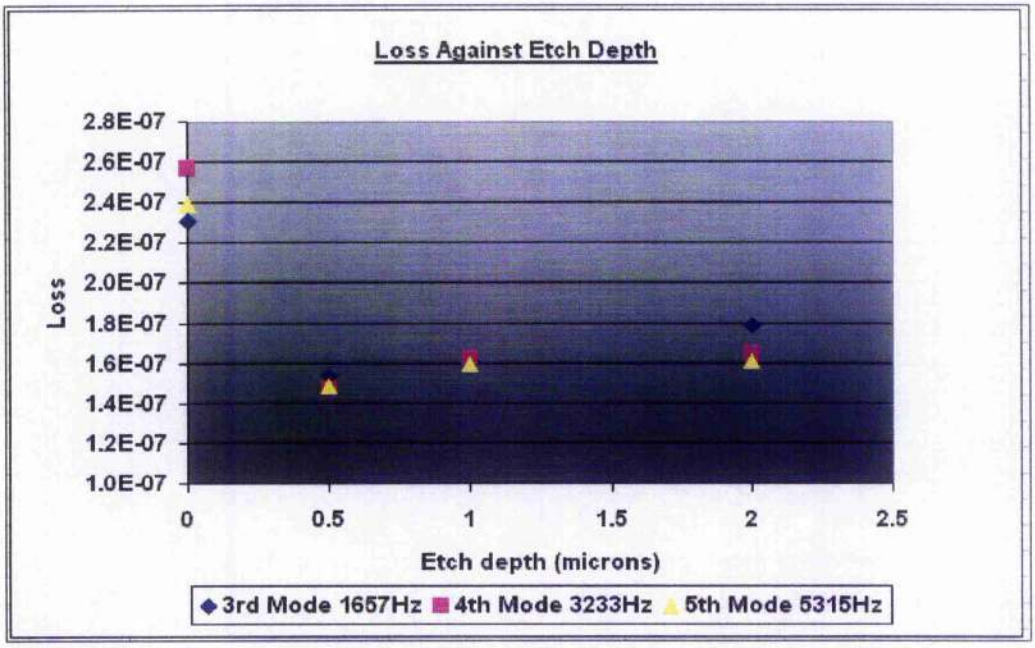

Figure 3.18: Loss as a function of etch depth, for modes 3,4 and 5.

Rather than plotting loss against frequency, loss as a function of etch depth is plotted in figure 3.18. Only modes three, four and five were considered because the first two modes may be suspension limited.

This produces a very interesting result: there is quite a large reduction in loss after the first 0.5 microns is removed. This implies that the lossy layer is a maximum of 0.5 microns deep. Etching more than 0.5 microns appears to result in an increase in the measured losses, some possible reasons for this are discussed later. Further investigation to see if the layer is shallower than this will have to be undertaken. However, if we assume for now that all of the loss due to the polishing is a result of some damaged layer that extends 0.5 microns into the surface, the loss associated with just this thin layer can be calculated. Also an altered surface loss term for the empirical model can be obtained for silica that has a 0.5 micron damaged surface layer due to polishing.

3.9 Estimate of the Mechanical Loss associated with a Polished (Damaged) Silica Surface Layer

First recall that Penn's equation for the total fused loss in silica can be decomposed into three terms:

$$\phi(f, \frac{V}{S}) = C_1(\frac{V}{S}) + C_2(\frac{f}{1Hz})^{C_3} + C_4\phi_{th} \tag{3.13}$$

For each of the modes of the cantilever, the values for each of these three terms is calculated and shown in table 3.8.

Frequency(Hz)	Bulk($C_2(\frac{f}{1Hz})^{C_3}$)	Surface Loss ($C_1(\frac{V}{S})$)	Thermo-elastic ($C_4\phi_{th}$)	Total - Surface
96	1.9×10^{-10}	2.98×10^{-8}	2.39×10^{-7}	2.39×10^{-7}
596	8.35×10^{-10}	2.98×10^{-8}	3.89×10^{-8}	3.98×10^{-8}
1657	1.92×10^{-9}	2.98×10^{-8}	1.40×10^{-8}	1.59×10^{-8}
3233	3.30×10^{-9}	2.98×10^{-8}	7.17×10^{-9}	1.05×10^{-8}
5315	4.95×10^{-9}	2.98×10^{-8}	4.36×10^{-9}	9.31×10^{-9}

Table 3.8: The predicted results for each of the terms in Steve Penn's Empirical Model (these numbers are obtained by plugging in the dimensions of our cantilever into the formula for the empirical model, equation 3.13).

In table 3.8, the total loss is calculated as the sum of the thermoelastic term plus the bulk loss term. For the moment, the contribution from the surface loss is not included - we want to calculate a new ϕ_s, for the case where the silica is polished.

The first step in the analysis, is to take the loss for each of the modes in the case where the cantilever is un-etched and subtract the loss measured for each mode after the 0.5 micron layer is etched from the surface. This improvement is attributed to the reduction in surface loss due to the damage in that 0.5 micron layer being etched away as shown in figure 3.19. Assuming this surface loss to be frequency independent, a new value for ϕ_s is obtained by taking the mean and standard deviation of these results.

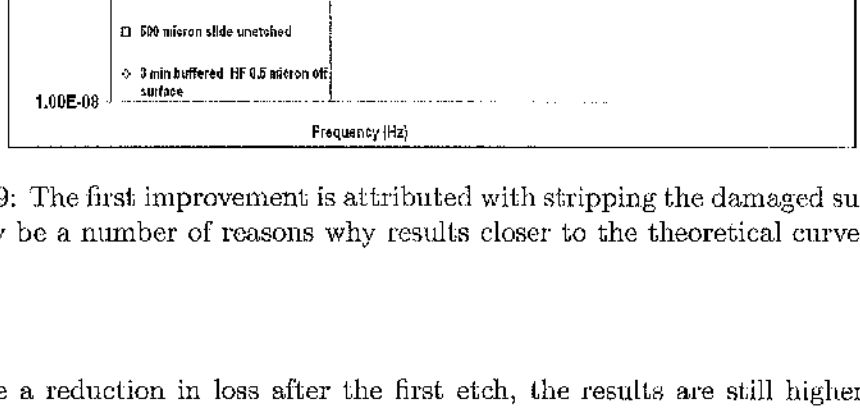

Figure 3.19: The first improvement is attributed with stripping the damaged surface away. There may be a number of reasons why results closer to the theoretical curve cannot be attained.

Despite a reduction in loss after the first etch, the results are still higher than predicted by the empirical model. Further etching of the cantilever yields higher losses. Some possible reasons for this are discussed later. In the next step, the difference between the lowest loss obtained (after the 0.5 layer is removed) and the empirical model is calculated. This difference is attributed to some other source of loss, such as recoil loss or loss due to stress or damage at the weld. This analysis is shown in table 3.9.

Frequency(Hz)	Calculated Surface Loss	Recoil Loss
96	2.43×10^{-6}	4.14×10^{-6}
596	-5.8×10^{-9}	1.17×10^{-7}
1657	7.76×10^{-8}	1.08×10^{-7}
3233	1.10×10^{-7}	1.07×10^{-7}
5315	9.01×10^{-8}	1.10×10^{-7}
Average (modes 3,4,5)	$9.25 \pm 0.93 \times 10^{-8}$	$1.08 \pm 0.01 \times 10^{-7}$

Table 3.9: The calculated surface and recoil losses for our sample (assuming that the additional excess loss is recoil).

Hence a new value for ϕ_s =9.25 $\times$ 10^{-8} is obtained. When compared to the current value (given by the empirical model) for cantilevers of this size, ϕ_s=2.98 $\times$ 10^{-8}, not surprisingly it is larger - by over a factor 3. It is also interesting rather than calculating a replacement term for Penn's equation, to calculate how lossy this layer is.

A simple model for the surface loss is based on the assumption that a surface layer of some thickness exists that uniformly exhibits a higher loss than the bulk of the material (consistent with Heptonstall et al, 2006). The loss of the surface layer itself, $\phi_{surface}$, is given by the measured surface loss, ϕ_s, multiplied by the ratio of the energy stored in the surface layer, $E_{surface}$, to the energy stored in the bulk of the cantilever, E_{bulk}, as it flexes:

$$\phi_s \approx \frac{E_{surface}}{E_{bulk}} \phi_{surface} \tag{3.14}$$

It is further shown in Heptonstall et al (2006):

$$\phi_s \approx \frac{3h}{a} \phi_{surface} \tag{3.15}$$

Where h is the thickness of the dissipative surface layer - 0.5 microns - and a is

the total thickness of our substrate, 500 microns. Note equation 3.15 is derived on the assumption that the Young's modulus of the surface is the same as for the bulk (there is some evidence that because of surface damage/pollutants etc it is effectively a different material and so it might be stiffer- but this possibility is not considered here). Equation 3.15 is rearranged and the values for ϕ_S given in table 3.9 are substituted for each mode. These results are shown in table 3.10. Again, assuming the surface loss is frequency independent, the mean surface loss is calculated.

Frequency(Hz)	Calculated Surface Loss In First 500 microns	$Q\ (\frac{1}{\phi})$
1657	2.59×10^{-5}	3.87×10^{4}
3233	4.67×10^{-5}	2.14×10^{4}
5315	3×10^{-5}	3.33×10^{4}
Average	$3.4 \pm 0.6 \times 10^{-5}$	$3.1 \pm 0.5 \times 10^{4}$

Table 3.10: Calculated loss for the first 0.5 micron surface layer of the studied 500μm thick cantilever.

3.10 Discussion and Conclusion

The constants used in the model from Penn et al, depend only on the type of silica used. However, the quality of the surface of the silica is clearly also important. It is found that measurements of silica with a high quality surface produce results that lie closer to those suggested by the model (Heptonstall et al, 2006). A new value for the model's surface term $\phi_s = 9.25 \times 10^{-8}$ is calculated for the case where the silica has been mechanically polished. This new value, when combined with the postulated levels of recoil, brings the model into line with the measured results after the first 0.5 micron etch. This was a factor three larger than the current value calculated for cantilevers of this size of ϕ_s=2.98×10^{-8}. The difference between these two values is most likely attributed to the fact that the ϕ_s in the empirical model is weighted by many of the samples having flame polished or flame

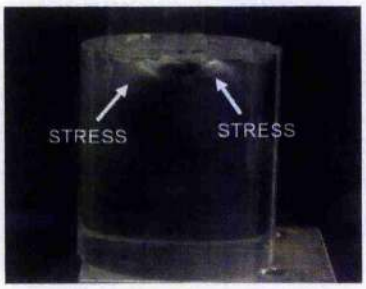

Figure 3.20: Stress (seen here through polarizers) around the weld area may be one reason why we can't get closer to the level of loss suggested by the empirical model.

pulled surfaces. Such surfaces are known to exhibit lower levels of loss (Penn et al, 2005).

The lossy layer of damage of a mechanically polished silica cantilever was found experimentally to extend up to 0.5 microns into the surface. The loss associated with this layer was calculated to be $3.4 \pm 0.6 \times 10^{-5}$. This is an important figure, because the silica test mass mirrors in interferometric gravitational wave detectors are also mechanically polished. This additional information will help when estimating the level of thermal noise in such a detector. However, further experimenting will need to be carried out to more accurately determine this number, because the results obtained show evidence of other sources of loss which require to be minimized.

One possible source of excess loss is material stress around the weld area between the cantilever and the test mass. When the weld area was examined through polarizers, a significant degree of stress is seen (see figure 3.20). Earlier the difficulties in welding two large silica samples was discussed, so welding losses may require improvements.

With regard to the experimental procedure, it is possible that the depth of damage due to polishing is less than 0.5 microns. The maximum possible improvement in loss by etching may have been "missed" if the further etching was degrading the surface quality

in some way, such as by chemical/structural damage. Conversely, it is possible the damaged layer may be *deeper* than 0.5 microns. Only a total of 2 microns was taken off the surface. It could be instructive to repeat the experiment with etching deeper in addition to etching in smaller increments. It may also be of interest to verify that the observed improvement in measured losses after etching was not as a result of some other effect.

For example, during the initial etch it is possible that other contaminants were removed from the surface such as silica dust deposited during the welding. This could account for the initial reduction in the measured loss. After this, further etching may have led to gradual and continual increase in surface loss.

The empirical model is weighted between silica with "pristine" surfaces. This kind of pristine surface can be achieved when silica is flame-drawn or flame polished. In addition, annealing silica may also improve the quality of its surface and hence significantly decrease the measured loss(Ageev et al, 2004). However, the attempt to fabricate these "ideal" silica surfaces, from mechanically polished substrates, through chemical etching was not completely achieved here. Further optimization of the etching procedure (perhaps by using different chemical etchants) may lead to further improvement in surface loss. It could be that, in the case of buffered HF, after an initial improvement, further etching may be causing chemical damage to the surface. Thus beyond an initial improvement, it is possible the losses will only increase.

In short, the results presented here suggest that the loss associated with a sub-micron damaged surface layer due to mechanical polishing, may be higher than current models for fused silica suggest.

Chapter 4

Investigations of the Mechanical Loss associated with Dielectric Optical Coatings

4.1 Introduction

In interferometric gravitational wave detectors the test mass and suspension elements consist of material with a low mechanical loss to reduce off-resonance thermal displacement noise. An important area of research is the development of the high reflectivity optical coatings for the test mass substrates. As this is the region where the laser beam is incident, dissipation from the coatings will contribute strongly to the thermal displacement noise. These coatings currently take the form of multilayered dielectric coatings.

A dielectric coating consists of a number of layers of alternating dielectric materials with different refractive indices. It is the varying indices of refraction (high and low) that give rise to the reflectivity of the coating. The coatings used in the initial interferometers were alternating $\frac{\lambda}{4}$ layers of silica and tantala (Ta_2O_5)(Harry et al, 2006). It

has been found that the tantala component of these coatings was the dominant source of the mechanical loss(Harry et al, 2006). One particular area of research is underway to minimize the mechanical loss of tantala through doping. Measurements made of single layer coatings of silica, tantala and doped tantala are discussed.

4.2 Uncoated Silica Cantilever Results

The results of measurements of the mechanical loss of seven un-coated silica cantilevers (0.11mm × 5mm × 45mm) are outlined. The cantilevers were measured in preparation for being coated with single layer coatings of silica, tantala and doped tantala by collaborators at LMA in Lyon, France. The mechanical loss of each cantilever is compared before and after it is coated. The increase in mechanical loss is then entirely attributed to the mechanical loss of the coating. Estimates of the mechanical loss in single layer coatings can help us to build a better picture of the losses associated with the multi-layer coatings in interferometric gravitational wave detectors.

Six of the samples were welded onto silica slides of approximate dimensions 10mm × 10mm × 1mm . A seventh sample was welded onto a thicker end piece (5mm thick). This was to investigate whether increasing the dimensions of the end piece resulted in a decrease in the measured loss, which might suggest some form of clamping losses. Since all of the cantilevers have approximately the same dimensions, the measured mechanical losses of the cantilevers should be likewise approximately the same. The results for these cantilevers are shown in figure 4.1.

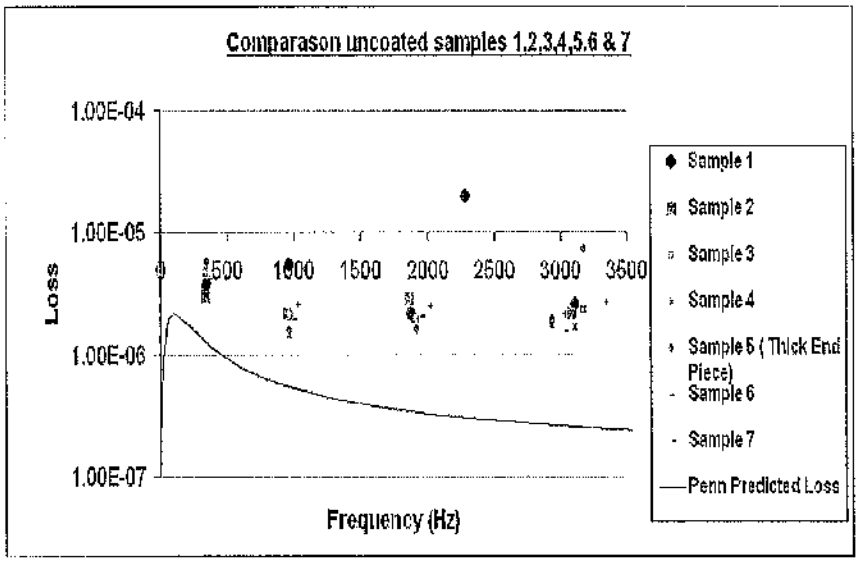

Figure 4.1: The measured losses of the seven uncoated silica cantilevers.

Small variations in the frequencies of the bending modes between each of the cantilevers were observed. The spread of frequencies is particularly noticeable at higher frequencies. The equation to predict the bending modes is given by 4.1:

$$w_n = (k_n l)^2 \frac{a}{2\sqrt{3}l^2} \tag{4.1}$$

From equation 4.1 there is a dependency on the frequency of the bending modes on the length (l) and thickness (a) of the cantilevers. Hence slight variations in the length and thickness of the samples are likely to account for the slight differences in the observed spread of frequencies of the bending modes.

From looking at 4.1, all of the cantilevers have approximately the same mechanical loss. Further, the cantilever welded to to the thicker end piece falls in line with the rest of the results, suggesting that clamping losses are unlikely to be dominating these measurements.

In sample 1 there is a mode at 2279 Hz that does not feature in the other samples. It is not a bending mode because it is not predicted by equation 4.1. It therefore must be some form of torsional mode. This mode, however, has a higher loss than all of the other modes by an order of magnitude. This is most likely due to energy coupling to the clamping structure for this particular mode. Such energy coupling can occur when the frequency of the resonant cantilever mode coincides with a resonance, or harmonic, of the clamp. Further investigation would be necessary here to determine the nature of the energy coupling, perhaps by using piezo transducers or finite element analysis.

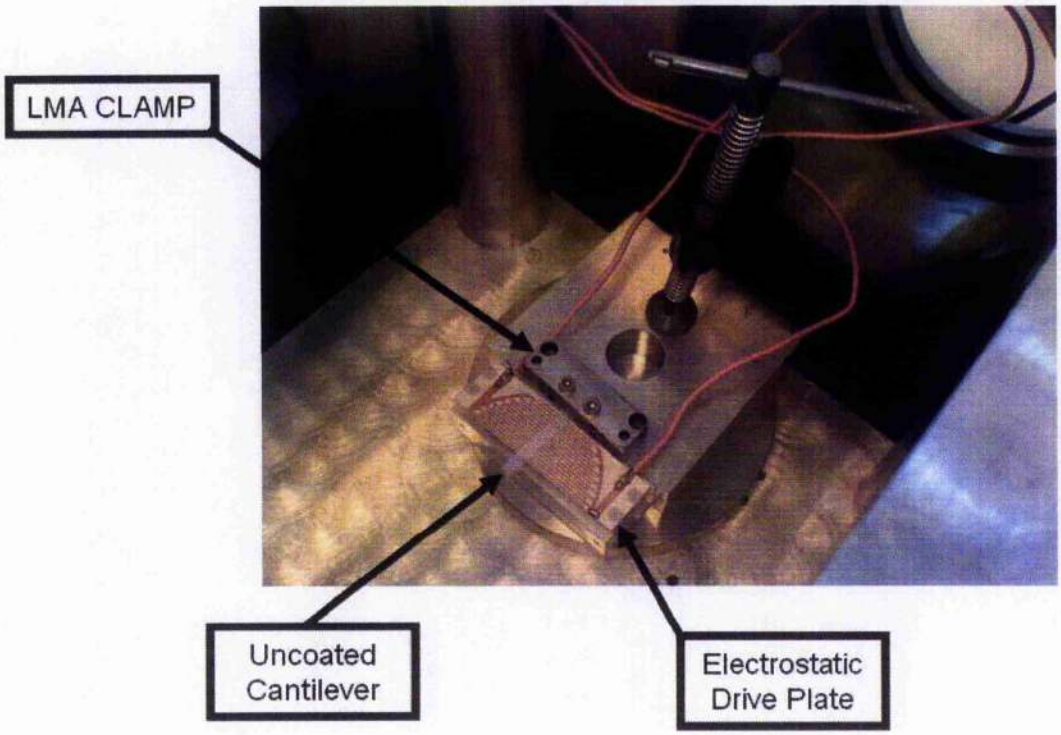

Figure 4.2: A picture of the LMA clamp in our tank

The mechanical loss of one further un-coated cantilever was measured. This cantilever was put in the LMA clamping system and then fixed in one of our vacuum tanks, see figure 4.2. In Glasgow, clamping losses are minimized by welding the cantilevers onto larger silica blocks which are clamped rigidly in place. In LMA, they do not have the facilities for flame or laser welding, so instead they focus on improving the clamp. It is interesting to compare the losses of an un-coated cantilever measured with our system and an un-coated sample measured by the LMA system. However, it should be noted that the clamps are prepared very carefully in France before a new sample is locked in place. The clamping surfaces are polished with very fine sandpaper.

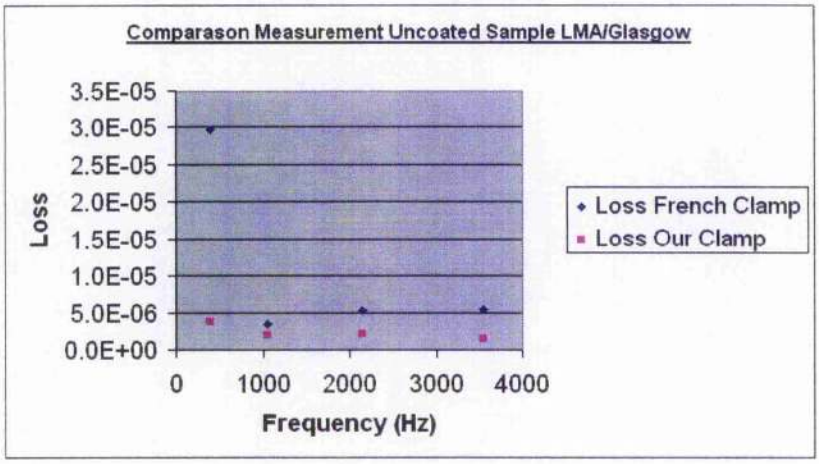

Figure 4.3: A comparison of the results obtained for the loss measurements of one of the uncoated cantilevers measured using the LMA and Glasgow systems. The mechanical loss for the fundamental mode in the LMA setup has a much higher loss which could suggest a problem with recoil loss for this setup.

4.3 Coated Silica Cantilevers Results

To calculate the coating losses, the energy ratios for each of the coated samples must be calculated. The Young's modulus of tantala (doped and undoped) was taken to be $\mathbf{Y}_{tantala} = \mathbf{1.4} \times \mathbf{10}^{11}$. The Young's modulus of silica is quoted as $\mathbf{Y}_{silica} = \mathbf{7.2} \times \mathbf{10}^{10}$. The coating is applied in a uniform 500 nm thick layer. The energy ratio is calculated using the formula:

$$E_R = 3\frac{Y_{coating}}{Y_{cantilever}} \times \frac{l_{coating}}{l_{cantilever}}$$

$l_{coating}$ is the thickness of the coating (500nm), $l_{cantilever}$ is the thickness of the cantilever 110μm (4.2)

Hence for each of the coatings the calculated energy ratio is shown in table 4.1

Tantala Doped	2.65×10^{-2}
Tantala Un-doped	2.65×10^{-2}
Silica	1.36×10^{-2}

Table 4.1: The calculated energy ratios for doped tantala, tantala and silica

Next the inverse of the energy ratios are multiplied by the difference in measured loss before and after the coating is applied. This gives a calculated value for the coating loss. The losses obtained for tantala, doped tantala and silica are given in tables 4.2, 4.3 and 4.4. They are compared in figure 4.4 on the next page.

Frequency	Coated	Un-coated	ϕ_δ	Coating Loss
2139	$(1.56 \pm 0.02) \times 10^{-5}$	$(5.190 \pm 0.008) \times 10^{-6}$	1.04×10^{-5}	3.93×10^{-4}
3543	$(1.740 \pm 0.004) \times 10^{-5}$	$(5.38 \pm 0.20) \times 10^{-6}$	1.20×10^{-5}	4.53×10^{-4}

Table 4.2: The calculated coating losses for a cantilever coated with a 500 nm thick layer of un-doped tantala.

Frequency	Coated	Un-coated	ϕ_δ	Coating Loss
2139	$(1.32 \pm 0.01) \times 10^{-5}$	$(5.190 \pm 0.008) \times 10^{-6}$	8.01×10^{-5}	3.02×10^{-4}
3543	$(1.32 \pm 0.01) \times 10^{-5}$	$(5.38 \pm 0.20) \times 10^{-6}$	7.82×10^{-5}	2.95×10^{-4}

Table 4.3: The calculated coating losses for a cantilever coated with a 500 nm thick layer of doped tantala.

Frequency	Coated	Un-coated	ϕ_δ	Coating Loss
2139	$(6.200 \pm 0.001) \times 10^{-6}$	$(5.190 \pm 0.008) \times 10^{-6}$	1.01×10^{-6}	7.41×10^{-5}
3543	$(7.00 \pm 0.01) \times 10^{-6}$	$(5.38 \pm 0.20) \times 10^{-6}$	1.62×10^{-6}	1.19×10^{-4}

Table 4.4: The calculated coating losses for a cantilever coated with a 500 nm thick layer of silica.

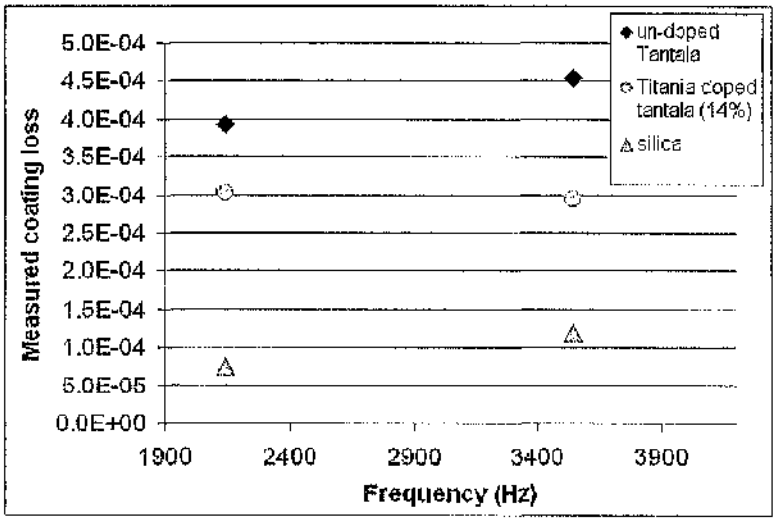

Figure 4.4: A comaparason of the coating losses of tantala, doped tantala and silica. Silica has the lowest measured coating loss. Doped tantala is observed to have a lower mechanical loss than in the undoped tantala.

The results presented here show that silica has the lowest coating loss overall and that doped tantala has a lower measured loss than case where the tantala is not doped. This is consistent with results presented elsewhere (e.g. Harry et al, 2006).

4.4 Estimation of Surface Loss associated with Un-Coated Samples (Polished, Annealed)

The un-coated samples measured are mechanically polished. It is interesting to compare the value obtained for the loss if this lossy layer is 0.5 micron deep as determined in the previous chapter. However, the comparison is not straightforward as these samples have been annealed. As discussed, it is found that annealing silica substrates can lead to a reduction in the measured mechanical loss.

First the average loss of the seven un-coated cantilevers is calculated. The difference between the average loss and the empirical model, the excess loss, could be attributed to surface loss associated with the mechanical polishing see table 4.4.

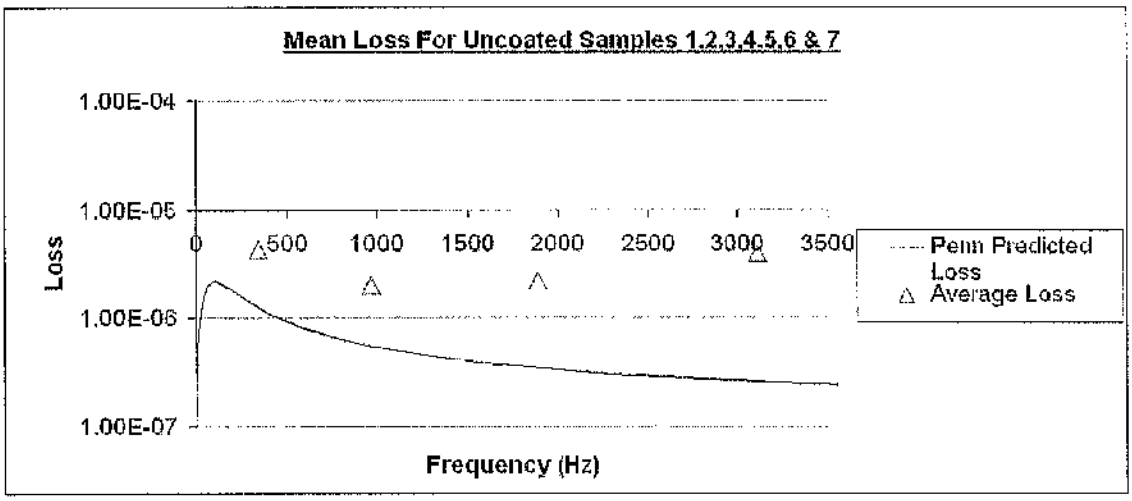

As with the coating losses, the excess loss, 3×10^{-6}, is multiplied by one over the energy ratio as given by equation 4.2 . The Young's modulus of the surface and the substrate are taken to be the same. This gives 2.1×10^{-4} for the loss attributed to mechanical polishing which is approaching a factor of approximately six higher than the value of 3.4×10^{-5}

Mode	Average Measured Loss	Empirical Model Predicted	Excess Loss
342	4.29×10^{-6}	9.81×10^{-8}	4.19×10^{-6}
963	1.99×10^{-6}	5.51×10^{-8}	1.93×10^{-6}
1890	2.16×10^{-6}	4.42×10^{-8}	2.12×10^{-6}
3106	3.96×10^{-6}	4.05×10^{-8}	3.92×10^{-6}
			Mean Excess Loss: 3.04×10^{-6}

Table 4.5: The difference between the average loss and the empirical model, the excess loss, could be attributed to surface loss associated with the mechanical polishing. The mean excess loss is calculated above.

obtained in chapter 3. This increased level of surface loss for these thinner samples could be attributed to a larger degree of surface damage/or thicker region of surface damage arising from the polishing of these particular samples.

4.5 Conclusions

Single layer coatings of silica, tantala and doped tantala were measured. It was found that the silica coating had the lowest level of measured mechanical loss overall at 3.77×10^{-5}. It was also found that doped tantala had a lower level of measured loss than tantala, 2.965×10^{-4} in the doped case compared to 4.24×10^{-4}.

Additionally seven un-coated samples were measured and they were found to have approximately the same level of loss ($\approx 10^{-6}$). The excess loss between the average value of the losses obtained from these cantilevers and the empirical model was determined. This excess loss was attributed to a 0.5 micron deep damaged surface layer due to mechanical polishing as determined in the previous chapter. The loss associated with this layer was found to be 2.1×10^{-4}, larger than value of 3.4×10^{-5} obtained in chapter 3. It was not known what effect the annealing process would have on the results presented in this chapter.

Chapter 5

Conclusions and Future Work

The results presented within this thesis show clearly that the level of mechanical loss associated with mechanical polishing of silica substrates may be higher than current models suggest. The damaged layer was estimated to be 0.5 micron deep with a loss of ϕ_s=2.98 $\times$ 10^{-8} which is three times higher than the surface loss predicted by the current empirical model. This is of importance when estimating the level of thermal noise in current and future gravitational wave detectors. The etching procedure presented allows improvements to be made to the mechanical loss associated with this mechanical polishing. However, as yet, these improvements did not bring the measured surface losses inline with the expected losses for surfaces associated with flame pulled or flame polished surfaces. Future work could be focussed on optimizing the etching conditions, such as investigating different chemical etchants, to achieve a higher quality surfaces. As also discussed, further studies using surface profiling may allow a link between surface loss and surface roughness to be evaluated. Mechanical loss studies of dielectric coatings was also undertaken. It was found that the silica coating had the lowest level of measured mechanical loss overall at 3.77×10^{-5}. It was also found doped tantala had a lower level of measured loss than tantala, 2.965×10^{-4} in the doped case compared to 4.24×10^{-4} when the tantala is undoped. Hence it was found that the tantala component is the dominant

source of mechanical loss and that this loss can be reduced by doping the tantala with titania. These results are consistent with previous measurements made here in Glasgow and by other groups around the world.

Bibliography

Chapter 1

J. Hough, S. Rowan, *Gravitational Wave Detection by Interferometry (Ground and Space)*, Living Reviews, **3** , 2000, 3.

K. Thorne, *Gravitational Waves*, arXiv.org:gr–qc/9506086, 1995.

L Ju et al, *Detection of gravitational waves*, Rep. Prog. Phys., **63** , 317-1427 , 2000.

D. Blair, *The Detection of Gravitational Waves*, Cambridge University Press, ISBN(10): 0521021022, 2005.

N. Roberston, *Laser Interferometric Gravitational Wave Detectors*, Class. Quantum Grav., **17** , R19-R40 , 2000.

V. Fafone, *Developments In Resonant Mass Detectors*, Class. Quantum Grav., **23** , S223-S229, 2006.

J. Hough, *Gravitational Waves- Principles of detection and an Overview of Detectors*, SIGRAV School, May 2005, http://www.physics.gla.ac.uk/~hough/PDFs/Singravlectures2.pdf

Chapter 2

A. Nowick, B. Berry, *Anelastic Relaxation in Crystalline Solids*, Materials Science Series, (Academic Press New York), 1972.

D. Crooks, *Mechanical Loss and its Significance in the Test Mass Mirrors of Gravitational Wave Detectors*, PhD Thesis, Glasgow University, 2003.

S. Reid, *Studies of Materials for Future Ground-Based and Space-Based Interferometric Gravitational Wave Detectors*, Phd Thesis, Glasgow University, 2006.

S. Penn, A. Ageev, D. Busby, G. Harry, A. Gretarson, K.Numata, P. Willems, *Frequency and surface dependence of the mechanical loss in fused silica*, arXiv.org:gr–qc/0507097, 2005.

Chapter 3

M. Kozlowski, J. Carr, I. Hutcheon, R. Torres, L. Sheenan, D. Camp, M. Yan, *Depth profiling of polishing-induced contamination on fused silica surfaces*, Proceedings of SPIE, Laser-Induced Damage in Optical Materials, edited by G. Exarhos, A. Guenther, M. Kozlowski, M. Soileau, 3244, 365-375, 1998.

J. Wiedersich, S. Adichtchev,E. Rossler, *Spectral Shape of relaxations in silica glass*, Physical Review Letters, 84, 12, 2000.

A. Heptonstall, G. Cagnoli, J. Hough, S. Rowan, *Characterisation of mechanical loss in*

synthetic fused silica ribbons, Physics Letters A, **354**, 353-359,2006.

A. Ageev, B. Palmer, A. Felice, S. Penn, P. Saulson, *Very high quality factor measured in annealed fused silica*, Quantum Grav., **21**, 3887-3892, 2004.

P. Caber, *Interferometric profiler for rough surfaces*, Applied Optics, **32**, pp. 3438, 1993.

M. Zecchino, E. Novak, J. Schmit, *Advances in Optical Profiling*, http://www.veeco.com

J. Bennet, J. Dancy, *Stylus profiling instrument for measuring statistical properties of smooth optical surfaces*, Applied Optics, **20**, p. 1785-1802, 1981.

C. Poon, B. Bhushan, *Comparison of surface roughness measurements by stylus profiler, AFM, and non-contact optical profiler*, Wear, **190**, pp. 76-78, 1995.

T. Quinn, C. Speake, R. Davis, W. Tew, Phys. Lett. A, **197**, 1995.

S.M. Twyford, PhD thesis, University of Glasgow, 1998.

H. Pain, *Physics of Vibrations and Waves*, Fifth Edition, John Wiley and Sons, ISBN 0 471 98543, 2000.

K. Khusnutdinova, D. Pelinovsky, *On the exchange of energy in coupled Klein-Gordon equations*, Wave Motion **38**, 1-10, 2003

Chapter 4

G. Harry, M. Abernathy, A. Becerra-Toledo, H. Armandula, E. Black, K. Dooley, M. Eichenfield, C. Nwabugwa, A. Villar, D. Crooks, G. Cagnoli, J. Hough, C. How, I. Maclaren, P. Murray, S. Reid, S. Rowan, P. Sneddon, M. Fejer, R. Route, S. Penn, P. Ganau, J. Mackowski, C. Michel, L. Pinard, A. Remilliex, *Titania-doped tantala/silica coatings for gravitional-wave detection.*, Class. Quantum Grav. **24**, 2006, 405-415.